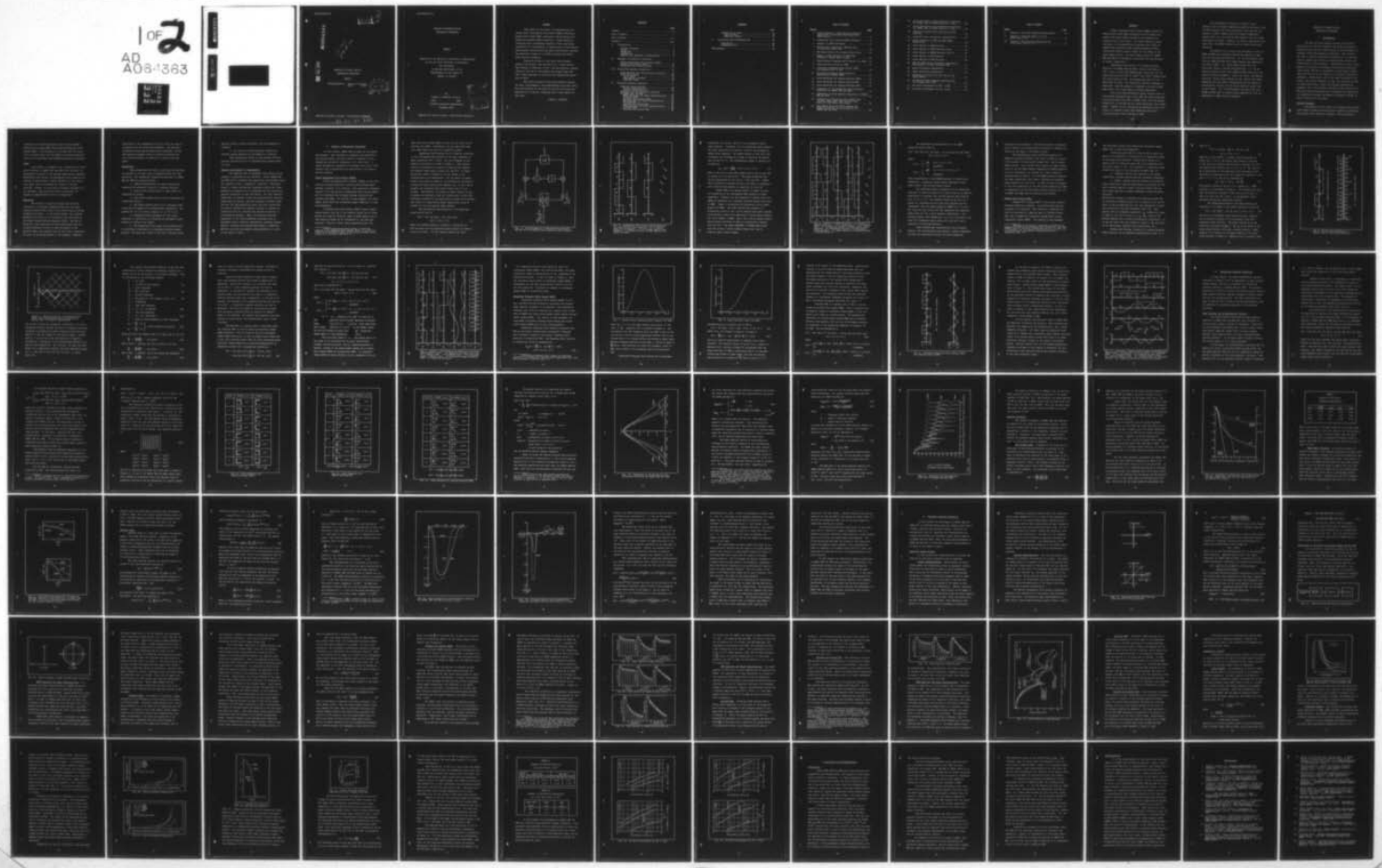
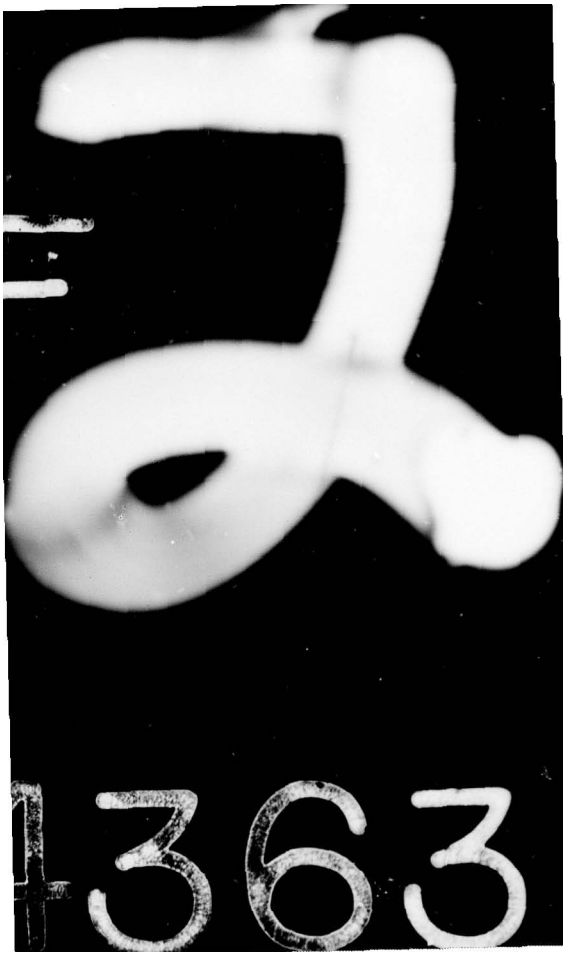
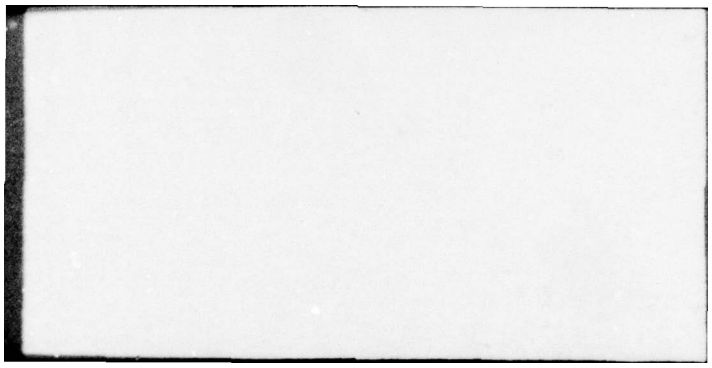
AD-A064 363 AIR FORCE INST OF TECH WRIGHT-PATTERSON AFB OHIO SCH--ETC F/G 9/3
ANALYSIS OF MODERN DIGITAL MODULATION TECHNIQUES.(U)
DEC 78 J L CRADDOCK

UNCLASSIFIED AFIT/GE/EE/78-23 NL

1 OF 2
AD A064363




363



AFIT/GE/EE/78-23

LEVEL II

AD A064363

See back page for 1473

DDC FILE COPY

ANALYSIS OF MODERN DIGITAL MODULATION TECHNIQUES

THESIS

AFIT/GE/EE/78-23 Joseph L. Craddock
Capt USAF

DDC
RECEIVED
FEB 9 1979
A

Approved for public release; distribution unlimited

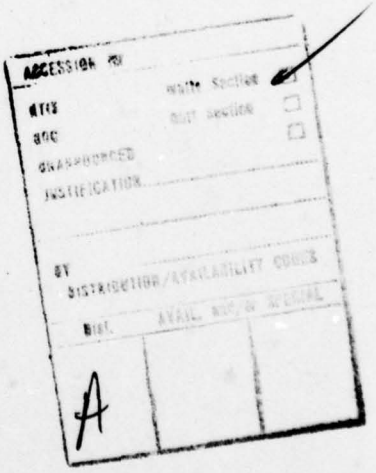
79 01 30 144

AFIT/GE/EE/78-23

ANALYSIS OF MODERN DIGITAL MODULATION TECHNIQUES

THESIS

Presented to the Faculty of the School of Engineering
of the Air Force Institute of Technology
Air University
in Partial Fulfillment of the
Requirements for the Degree of
Master of Science



by
Joseph L. Craddock, B.T.E.T.
Capt USAF
Graduate Electrical Engineering
December 1978

Approved for public release; distribution unlimited

Preface

This report is the result of evaluating and comparing Offset Quadriphase Shift Keyed (OQPSK) modulation, Minimum Shift Keyed (MSK) modulation, and Sinusoidal Frequency Shift Keyed (SFSK) modulation. These modulation techniques were investigated because of their particular suitability for transmission of digital data in environments where system nonlinearities and power efficiencies constrain the modulation format to a constant envelope and narrow power spectral bandwidth.

During the course of this work, much valuable guidance and insight was provided by my thesis advisor Capt Stanley R. Robinson; to him I am most grateful. Special thanks is also due to the readers Capt Gregg Vaughn and Capt Frank Kirschner of the Electrical Engineering Department of AFIT.

This project would not have been possible without the help, encouragement, and understanding of my wife, Rita. Her unselfishness for the past two and one half years has permitted me to achieve a personal goal I have wanted for some time.

Joseph L. Craddock

Contents

	Page
Preface	ii
List of Figures	v
List of Tables	vii
Abstract	viii
I. Introduction	1
Problem Statement	1
Scope	2
Background	2
Assumptions	3
Approach and Sequence of Presentation	4
II. Analysis of Modulation Techniques	5
Offset Quadriphase Shift Keying (OQPSK)	5
Minimum Shift Keying (MSK)	12
Sinusoidal Shift Keying (SFSK)	21
III. Theoretical Spectral Properties	28
Power Spectrum and Autocorrelation Function	28
Spectral Occupancy	40
Out-of-Band	40
Mean-Square Crosstalk	43
Spectral Shape	45
IV. Practical Spectral Properties	53
Practical System Devices	53
Filter Characteristics	53
Limiter Characteristics	54
Application of Filtering and Limiting to OQPSK, MSK and SFSK	57
OQPSK Amplitude and Phase Characteristics	58
Filtered OQPSK	59
Filtered and Limited OQPSK	62
MSK Amplitude and Phase Characteristics	65
Filtered MSK	65
Filtered and Limited MSK	66
SFSK Amplitude and Phase Characteristics	67
Filtered SFSK	69
Filtered and Limited SFSK	69

Contents

		Page
	Probability of Error	70
	Ideal Channel	70
	Realistic Channel	71
V.	Conclusions and Recommendations	80
	Conclusions	80
	Recommendations	83
	Bibliography	84

List of Figures

Figure		Page
1	Block Diagram of a QPSK Modulator Realized Through Two Overlapping Phase Quadrature BPSK Channels	7
2	Quadriphase Shift Keying (QPSK) Waveforms	8
3	Example of OQPSK Waveforms.	10
4	Minimum Shift Keying as a Special Case of Continuous Phase FSK	15
5	MSK Phase Trellis for Possible Phase Paths	16
6	Example of MSK Waveform as OQPSK With Sinusoidal Shaped Symbol Pulses	20
7	Raised-Cosine Frequency Shift Function for SFSK	22
8	Phase Deviation Curve for SFSK	23
9	Sinusoidal Frequency Shift Keying (SFSK) as a Special Case of FSK.	25
10	Sinusoidal Frequency Shift Keying as Raised-Cosine Shaped OQPSK	27
11	State Waveforms for Complex Envelope OQPSK	32
12	State Waveforms for Complex Envelope MSK	33
13	State Waveforms for Complex Envelope SFSK	34
14	Comparison of the Normalized Autocorrelation Functions for OQPSK, MSK and SFSK	36
15	Comparison of Power Spectral Densities for OQPSK, MSK and SFSK	39
16	Comparison of Fractional Out-of-Band Power for PSK, OQPSK, MSK, SFSK and the Lower Bound for Any Symbol Pulse Shape	42
17	Mean-Square Crosstalk $E(C^2)$ Between Two Adjacent Channels of Like Modulation for OQPSK, MSK and SFSK	44

18 First Derivative of Autocorrelation Functions for OQPSK, MSK and SFSK (Positive τ Only) 48

19 Second Derivative of Autocorrelation Functions for OQPSK, MSK and SFSK (Positive τ Only) 49

20 Comparison Between Hard Limiting and Soft Limiting 55

21 Combined Filter and Limiter Configuration 57

22 Phasor Diagrams of BPSK and QPSK Phase Transitions 58

23 Power Spectra of QPSK Envelope 64

24 Power Spectra of OQPSK Envelope (BT=1) 64

25 Power Spectra of OQPSK Envelope (BT=0.5) 64

26 Power Spectra of MSK Envelope 67

27 Power Spectrum of MSK Envelope 68

28 MSK and OQPSK E_b/N_o Performance Degradation With Respect to Ideal Antipodal PSK 71

29 E_b/N_o Performance Degradation 73

30 E_b/N_o Performance Degradation 73

31 Probability of Error for BT=1.3R and 1dB Input Backoff 74

32 Voltage and Phase Transfer Characteristic for a Hughes 261-H TWT 75

33 Bit Error Performance for BT = 1.08R 78

34 Bit Error Performance for BT = 0.81R 79

List of Tables

Table		Page
I	Summary of Two Sided Bandwidth Requirements . . .	43
II	Summary of Required E_b/N_o for a Bit Error Rate of 10^{-5}	77
III	Summary of Differential Degradation for a Bit Error Rate of 10^{-5}.	77

Abstract

Offset Quadriphase Shift Keyed (OQPSK) modulation, Minimum Shift Keyed (MSK) modulation and Sinusoidal Frequency Shift Keyed (SFSK) modulation are analyzed and compared within this report. The three modulation types are shown to be mathematically identical when viewed as inphase and quadrature phase channels employing offset, time-shifted symbol pulses, except for the shapes of the input symbol pulses. The input symbol pulses for OQPSK, MSK and SFSK are rectangular, sinusoidal and raised-cosine in shape, respectively.

Theoretical calculations of the power spectral densities for OQPSK, MSK and SFSK reveal first nulls at $f/R = 0.50$, 0.75 and 0.86 respectively, while the roll off characteristics are $(f/R)^{-2}$, $(f/R)^{-4}$ and $(f/R)^{-8}$ respectively for large values of f/R. The normalizing term R is the input data bit rate. The theoretical spectral occupancy of each power spectral density is computed by an out-of-band power ratio, and a mean-square crosstalk calculation.

The out-of-band performance curves indicate that for a BT product exceeding about 3.0R, SFSK has lower fractional out-of-band power than MSK or OQPSK, while for a BT product between 3.0 to 1.5R MSK has the lowest fractional out-of-band power. However, as the BT product is decreased below 1.0R, a point is reached ($\approx$0.7R) where OQPSK has fractional out-of-band power lower than MSK or SFSK.

The mean-square crosstalk performance curves indicate that for channel separations greater than about 2.3R, two SFSK channels have less mean-square crosstalk than two channels of MSK or OQPSK, while for channel separations between about 0.75 and 2.3R two MSK channels have the lowest mean-square crosstalk. However, for channel separations less than 0.75R, two OQPSK channels have the lowest mean-square crosstalk.

An analysis of bit error rate performance curves for OQPSK and MSK from nonlinear bandlimited channels is made with the following observations: (1) For BT products less than 2R, OQPSK and MSK offer significantly less degradation than PSK or QPSK. (2) Offset QPSK and MSK are both relatively immune to system nonlinearities. (3) For BT products between 2R and 0.6R, OQPSK and MSK offer about the same bit error performance. Various bit error performance crossover points exist between the two within this range depending upon the system configuration and the degree of nonlinearity; however, the bit error rates are within 1dB of each other. (4) For BT products less than 0.6R, both OQPSK and MSK begin to suffer severe degradation, with the degradation of MSK being the greatest.

ANALYSIS OF MODERN DIGITAL MODULATION TECHNIQUES

I Introduction

The need for good spectrum economy and efficient utilization of available bandwidth has caused considerable interest within the last several years in the development of advanced coding and modulation techniques. This interest has lead to numerous theoretical analyses and to a proliferation of papers and articles in communication journals and transactions on these subjects. Unfortunately, most of these papers and articles are primarily theoretical and mathematically based, and due to limitations in publication length, only deal with one or two aspects of a coding or modulation technique. Additionally, due to the rapid evolution of the theory, very little treatment, if any, can be found in books or textual materials. Hence, the working communication engineer, who is not directly involved in this evolution but who needs detailed and practical information for application to a particular problem, can expend considerable energy and time in arriving at a solution.

Problem Statement

The purpose of this thesis is to examine and evaluate three modern constant-envelope digital modulation techniques with minimum power spectral occupancy. These modulation

techniques are Offset Quadriphase Shift Keying (OQPSK), Minimum Shift Keying (MSK) and Sinusoidal Frequency Shift Keying (SFSK). The analysis is to be made with the objective of establishing a set of practical operating characteristics to be considered when choosing modulation techniques.

Scope

This thesis is intended to be a compilation of available literature on OQPSK, MSK and SFSK, with the level of presentation directed to the working communication engineer. Mathematical derivations and explanations will primarily be limited to establishing a common framework for the modulation types, and in evaluating the content of various articles. However, in cases where necessary information is not available, some derivations will be included. No testing or experimentation will be accomplished.

Background

The interest in spectrum economy and efficient utilization of available bandwidth stems from the rapid expanding communication needs of our society and an already crowded RF spectrum. In the United States, the occupied bandwidth and efficiency of utilization are controlled by the Federal Communications Commission (FCC). The FCC in Docket No. 19331 specifies for LOS transmissions that the occupied bandwidth contain at least 99 percent of the spectral power, and requires that not more than 1 percent of the power be contained outside of the assigned bandwidth.

Additionally, the transmission bit rate R must be equal to or greater than the authorized bandwidth. For LOS radio transmission using digital modulation techniques, the FCC also specifies maximum levels of spectral densities for out-of-band emissions, in addition to total out-of-band power.

Assumptions

Many assumptions were made in defining and narrowing the problem to one that could be analyzed within the time permitted. The fundamental assumptions applicable to OQPSK, MSK and SFSK are presented below:

1. System nonlinearities and power efficiencies constrain the modulation format to a constant envelope.

2. Hard or soft limiters will be used within the communication system.

3. Only binary digital data is used to modulate the transmitted carrier.

4. The binary digital data is in a continuous data stream and is assumed to be statistically independent. The probability of a bit being a logical "1" or "0" is 1/2.

5. Transmitted waves propagate in free space; therefore, no distortion is introduced by atmospheric interference or fading of the signal.

6. The predominant noise added to the signal prior to filtering is described as a stationary Gaussian random process. The noise has a mean of zero and a two-sided power

spectral density of $N_o/2$ (watts/Hz) over the bandwidth of interest.

7. All levels of synchronization required for complete system operation are available at a receiver.

Other assumptions needed to help resolve the mathematical derivations will be presented where needed within the text.

Approach and Sequence of Presentation

The approach used to accomplish this thesis and the sequence of presentation are identical. First, OQPSK, MSK and SFSK will be examined both graphically and mathematically, and compared to more fundamental modulation techniques. Second, a common mathematical framework unifying the three modulation techniques will be developed and the theoretical spectral properties of each calculated. The term "spectral properties" is defined to mean the autocorrelation function, power spectral density, spectral occupancy, spectral shape and roll off characteristics; while the term "theoretical" is used to indicate that filters, limiters or system nonlinearities have not modified the spectral properties of the modulated waveform. Next, the practical spectral properties of the three modulation techniques will be developed using a realistic bandlimited, nonlinear channel. Finally, simulated and measured performance of OQPSK and MSK will be given and compared using probability of error as the figure of merit.

II Analysis of Modulation Techniques

In this chapter, OQPSK, MSK and SFSK are introduced and analyzed. Each technique is examined both graphically and mathematically, and where possible, compared to more fundamental modulation techniques, or to each other. A common mathematical framework is developed as an aid in this analysis and in preparation for calculations to be made in further chapters.

Offset Quadriphase Shift Keying (OQPSK)

Offset Quadriphase Shift Keying[1] (OQPSK) is the first constant-envelope modulation technique with minimum power spectral occupancy to be analyzed. This modulation technique, because of its similarity to Quadriphase Shift Keying (QPSK), will be introduced and developed through comparison and contrast with QPSK. For clarity of some passages, the terms OQPSK, Offset QPSK and rectangular shaped OQPSK will be used interchangeably.

In binary Phase Shift Keying (BPSK) digital communication system, only one of two possible phases can be transmitted in a data bit interval, while in QPSK system, one of four possible phases can be transmitted in the same time interval. Thus for a given output signalling rate, the

---

[1]Offset Quadriphase Shift Keying is sometimes referred to as Staggered QPSK (SQPSK) (Refs. 1, 2, and 3), Offset Keyed Quadrature Phase Shift Keying (OK-QPSK) (Refs. 4 and 5), or as Offset PSK (Ref. 6).

input data rate through QPSK is twice the rate that can be achieved with BPSK. Alternately, for the same input data rate, QPSK needs only half the bandwidth as BPSK.

Quadriphase Shift Keying can be viewed as consisting of two overlapping BPSK channels of the same frequency in phase quadrature (Ref. 7:333). The block diagram of this parallel realization is shown in Figure 1. Each channel carrier is modulated by a series of positive and negative rectangular shaped symbol pulses C(t) and S(t), of length 2T seconds, where T seconds is the bit length of the incoming data to be transmitted. The two series of symbol pulses illustrated in Figure 2, are obtained by alternately routing the input bipolar data sequence, d_k, to the I and Q channels and extending their pulse length from T to 2T seconds. Additionally, the series of symbol pulses for the Q channel are delayed in time by T seconds for a total time difference between the two symbol pulse streams of 2T seconds. This results in simultaneous phase transitions, every 2T seconds for the two parallel BPSK channels.

The mathematical representation of the QPSK modulated carrier wave is

$$Y(t) = C(t) \text{ Cos } (W_c t) + S(t) \text{ Sin } (W_c t)$$
$$kT \leq t \leq (k + 1) T \qquad (1)$$

where the inphase channel (I channel) is identified as C(t) Cos (W_ct) and the quadrature phase channel (Q channel) as S(t) Sin (W_ct). For the inphase channel Cos (W_ct)

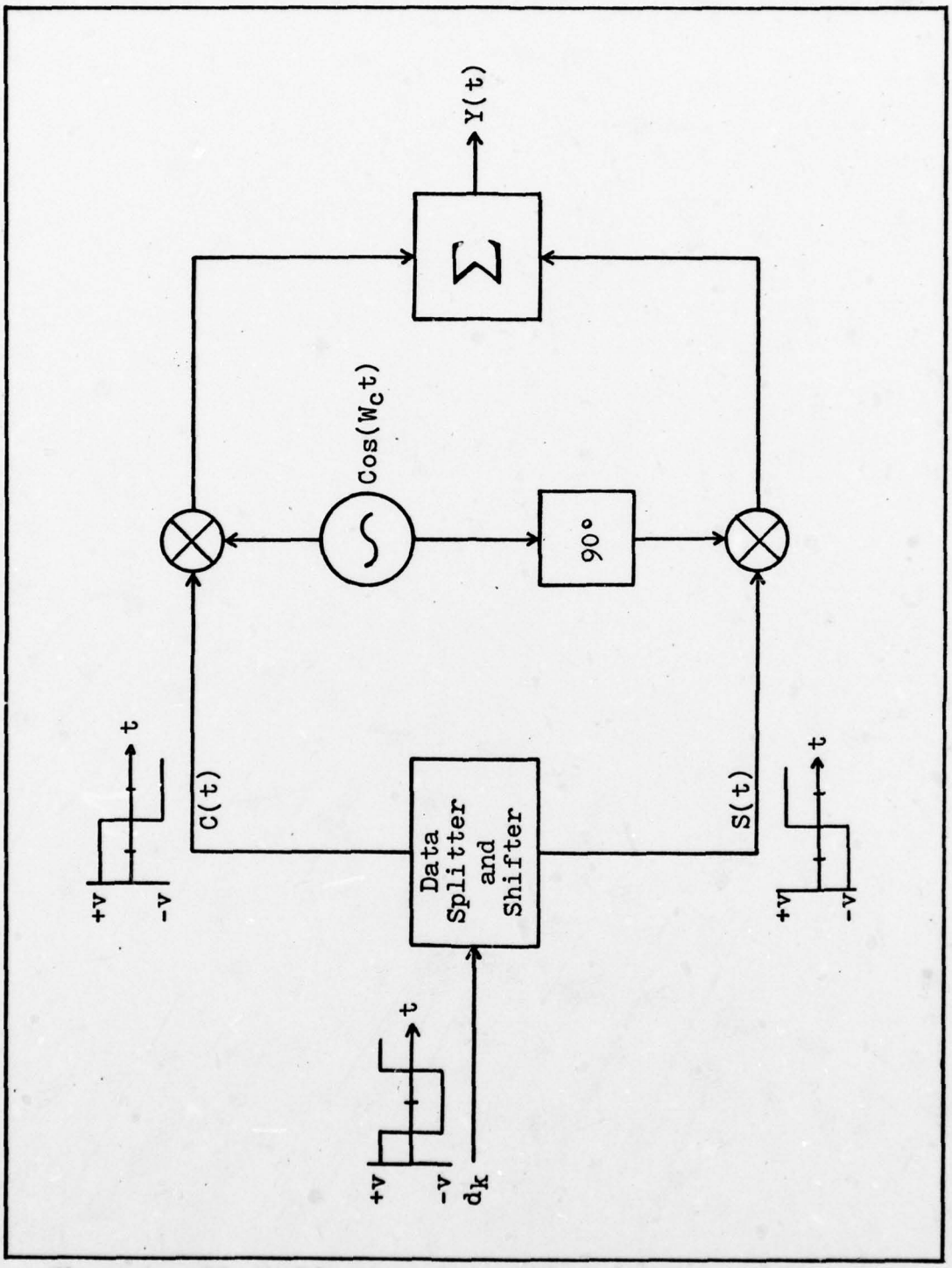


Fig. 1. Block Diagram of a QPSK Modulator Realized Through Two Overlapping Phase Quadrature BPSK Channels.

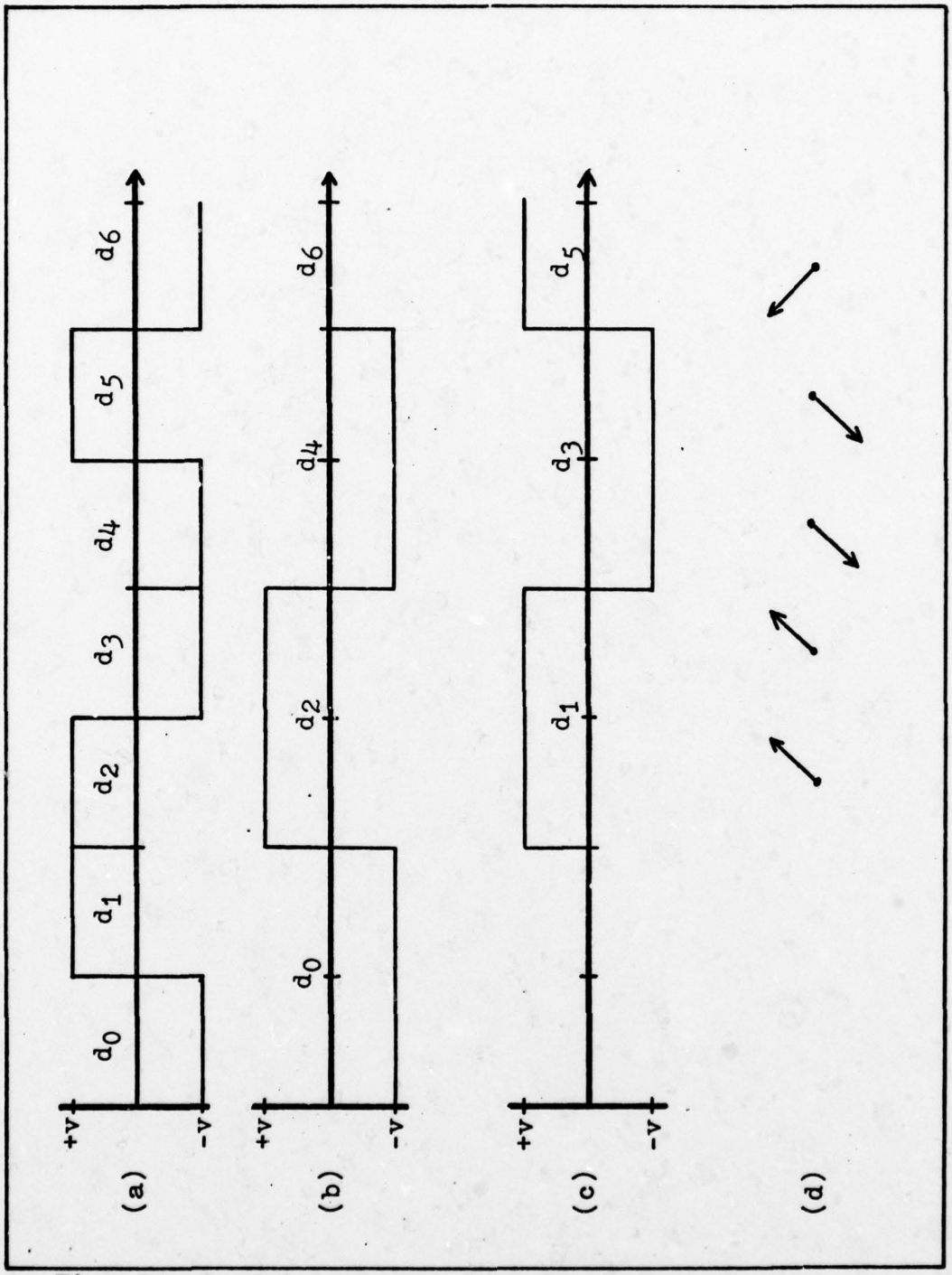


Fig. 2. Quadriphase Shift Keying (QPSK) Waveforms. (a) Input Bipolar Data Sequence. (b) I Channel Symbol Pulse Sequence. (c) Q Channel Symbol Pulse Sequence. (d) Phase Deviation of QPSK Waveform in Phasor Notation.

represents the carrier, and C(t) the rectangular symbol pulse sequence. Similarly, for the quadrature phase channel, Sin ($W_c t$) represents the carrier, and S(t) the rectangular symbol pulse sequence. The symbol pulses in both the I and Q channels are rectangular in shape of duration 2T seconds with values of ± 1. The instantaneous phase of equation (1) is given by

$$\theta_d = \tan^{-1} \frac{S(t)}{C(t)}, \quad kT \leq t \leq (k + 2)\ T \qquad (2)$$

where k can take on only odd integer values, and θ_d can take on values of ± 45° and ± 135°. The phase deviations that can be represented by this are 0°, ± 90° and 180°. Figure 2(d) illustrates by phasor notation the result of applying a given bipolar data sequence to equations (1) and (2).

Offset QPSK, in a manner similar to QPSK, can also be represented as two overlapping BPSK channels in phase quadrature. However, the two sequences of symbol pulses for OQPSK are generated in a slightly different manner than those of QPSK. Figure 3 illustrates the generation of the symbol pulses for OQPSK. The input bipolar data sequence is alternately routed to the I and Q channels with pulse lengths of 2T seconds, without the additional T second delay required for the Q channel of QPSK. Next, the I and Q channels symbol pulse streams alternate in sign as illustrated in Figures 3(d) and 3(e). The names STAGGERED or OFFSET QPSK result from the natural T second offset between the I and Q channels symbol pulse streams.

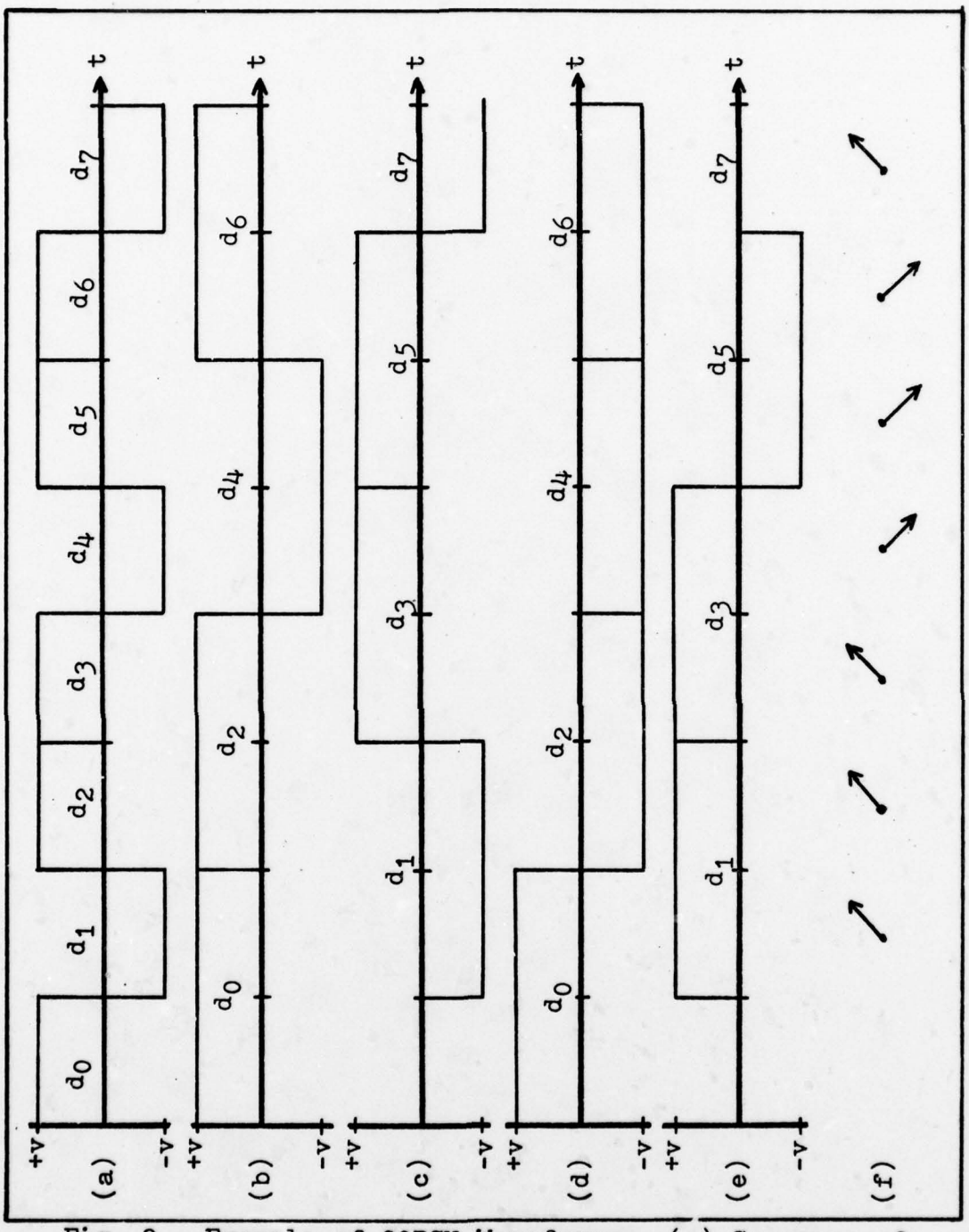


Fig. 3. Example of OQPSK Waveforms. (a) Sequence of Bipolar Data (d_k). (b) I Channel Data. (c) Q Channel Data. (d) Rectangular Shaped I Channel Symbol Pulse Sequence. (e) Rectangular Shaped Q Channel Symbol Pulse Sequence. (f) Phase Deviation of OQPSK Waveform in Phasor Notation.

The mathematical representation of the OQPSK modulated carrier wave is

$$Y(t) = \text{Cos}\,(X_k)\; C(t)\; \text{Cos}\,(W_c t) - d_k\; \text{Cos}\,(X_k)\; S(t)\; \text{Sin}\,(W_c t)$$
$$kT \le t \le (k+1)\,T \qquad (3)$$

where

$$C(t) = \begin{cases} \frac{1}{\sqrt{2}} & kT \le t \le (k+2)\,T \\ 0 & \text{elsewhere} \end{cases}$$

$$S(t) = \begin{cases} \frac{1}{\sqrt{2}} & (k-1)\,T \le t \le (k+1)\,T \\ 0 & \text{elsewhere} \end{cases}$$

This representation of the OQPSK waveform is viewed as an inphase and a quadrature phase channel employing rectangular offset, time-shifted symbol pulses.

The individual parts of equation (3) are identified similarly to those of equation (1) except that X_k is additive phase which is constant over the kth bipolar data interval $kT \le t \le (k+1)\,T$. The possible values of X_k are 0 or π, modulo 2π, determined by the input data sequence and the requirement that the phase change for OQPSK be 0° or ± 90°. The terms $\text{Cos}\,(X_k)$ and $d_k\,\text{Cos}\,(X_k)$ represent data dependent phase terms for the I and Q channels respectively. The incoming bipolar data stream $\{d_k = \pm 1\}$ is at the rate $R = \frac{1}{T}$, with the rectangular symbol pulses for both the I and Q channels of 2T seconds duration.

Other mathematical representations are available, however, this representation was chosen to permit comparison and show the commonality between the three modulation

techniques being analyzed. The other modulation techniques will be shown to be mathematically identical to equation (3) except for the shape of the symbol pulses.

The instantaneous phase deviations possible for OQPSK are slightly different than those of QPSK as a result of the natural T second offset between the I and Q channel symbol pulses. The T second offset causes the phase transitions of the two BPSK channels composing the OQPSK modulator to occur alternately, one channel at a time, instead of simultaneously as before. For the OQPSK modulated waveform, the phase transitions occur every T seconds with possible phase changes of 0° and ± 90°. It will be shown in Chapter 4, that the elimination of the 180° phase transition of QPSK is responsible for the more rapid spectral density roll off of OQPSK than QPSK when filtered and hard limited.

Minimum Shift Keying (MSK)

Minimum Shift Keying (MSK)[2] is the second constant-envelope modulation technique with minimum power spectral occupancy to be analyzed. This modulation technique will first be developed as a special case of continuous phase FSK, then as OQPSK with sinusoidal shaped symbol pulses (sinusoidal shaped OQPSK). For clarity of some passages,

[2]Minimum Shift Keying is sometimes referred to as Minimum (Frequency) Shift Keying (Refs. 9 and 10), Fast FSK (FFSK) (Ref. 6), FSK with modulation index of 0.5 (Ref. 11), or as FM-PSK with rectangular frequency modulation signalling (Ref. 12).

the terms MSK, Minimum Shift Keying and sinusoidal shaped OQPSK will be used interchangeably.

Continuous phase FSK is a form of FSK in which the phase of the waveform is continuous at the transition points of the signalling intervals. Minimum Shift Keying is a special case of continuous phase FSK, with frequency deviation ratio equal to 1/2. The constraint of continuous phase effects the signal in the following two ways (Ref. 8):

1. Transient affects are lessened at the symbol transitions, thereby offering spectral bandwidth advantages.

2. Memory, imposed upon the waveform by continuous phase transitions, improves performance by providing for the use of several symbols to make a decision rather than the more common approach of making independent symbol-by-symbol decisions.

Minimum Shift Keying is obtained from continuous phase FSK by utilizing a frequency shift, f_s, of exactly $\pm$ 1/4 the bit rate, R, and by requiring that the tone frequencies be exact even multiples of the shift frequency (Ref. 13). This implies that the frequency separation, f_Δ, between the tones, is equal to 1/2 the bit rate (i.e. $f_\Delta = \frac{R}{2}$). This is the minimum spacing that provides orthogonality (correlation = 0) of the two tones over the interval T, where $T = \frac{1}{R}$, and leads to the terminology "Minimum" Shift Keying (Ref. 14).

Minimum Shift Keying, treated as a constant-envelope CPFSK waveform, can be expressed mathematically (Refs. 4, 5,

and 15) as

$$Y(t) = \text{Cos}\left[W_c t + \frac{\pi}{2T}(t - kT)\, d_k + X_k\right]$$

$$kT \le t \le (k + 1)\, T \qquad (4)$$

where W_c is the carrier, or center, radian frequency in rad/s, $\{d_k = \pm 1\}$ is the bipolar data stream at the rate $R = \frac{1}{T}$, and X_k is additive phase which is constant over the kth bipolar data interval $kT \le t \le (k + 1)\, T$. The value of X_k is determined by the requirement that the phase of the waveform be continuous at the bit transition instants $t = kT$ and $t = (k + 1)\, T$, and can be expressed as

$$X_k = X_{k-1} + (d_{k-1} - d_k)\frac{\pi k}{2} \qquad (5)$$

The possible values of X_k are 0 or π, modulo 2π. A MSK waveform is illustrated in Figure 4. The convention is used that the modulator transmit a high tone (f_h) for data + 1 and a low tone (f_l) for a data - 1, and generate cosine waveforms during each signalling interval.

The instantaneous phase of the MSK waveform with reference to the phase of the carrier waveform is given by

$$\theta(t) = X_k + \frac{\pi}{2T}(t - kT)\, d_k,\ kT \le t \le (k + 1)\, T \qquad (6)$$

thus $\theta(t)$ is a piecewise linear phase function. Equation (6) is plotted in Figure 5 for all possible input data sequences (phase trellis). The phase constant X_k is the phase axis intercept and $\frac{\pi}{2T}(t - kT)\, d_k$ is the slope of the linear phase function over each T second interval. Superimposed on the trellis is the phase function of the modulated waveform of Figure 4. Figures 4 and 5 illustrate that

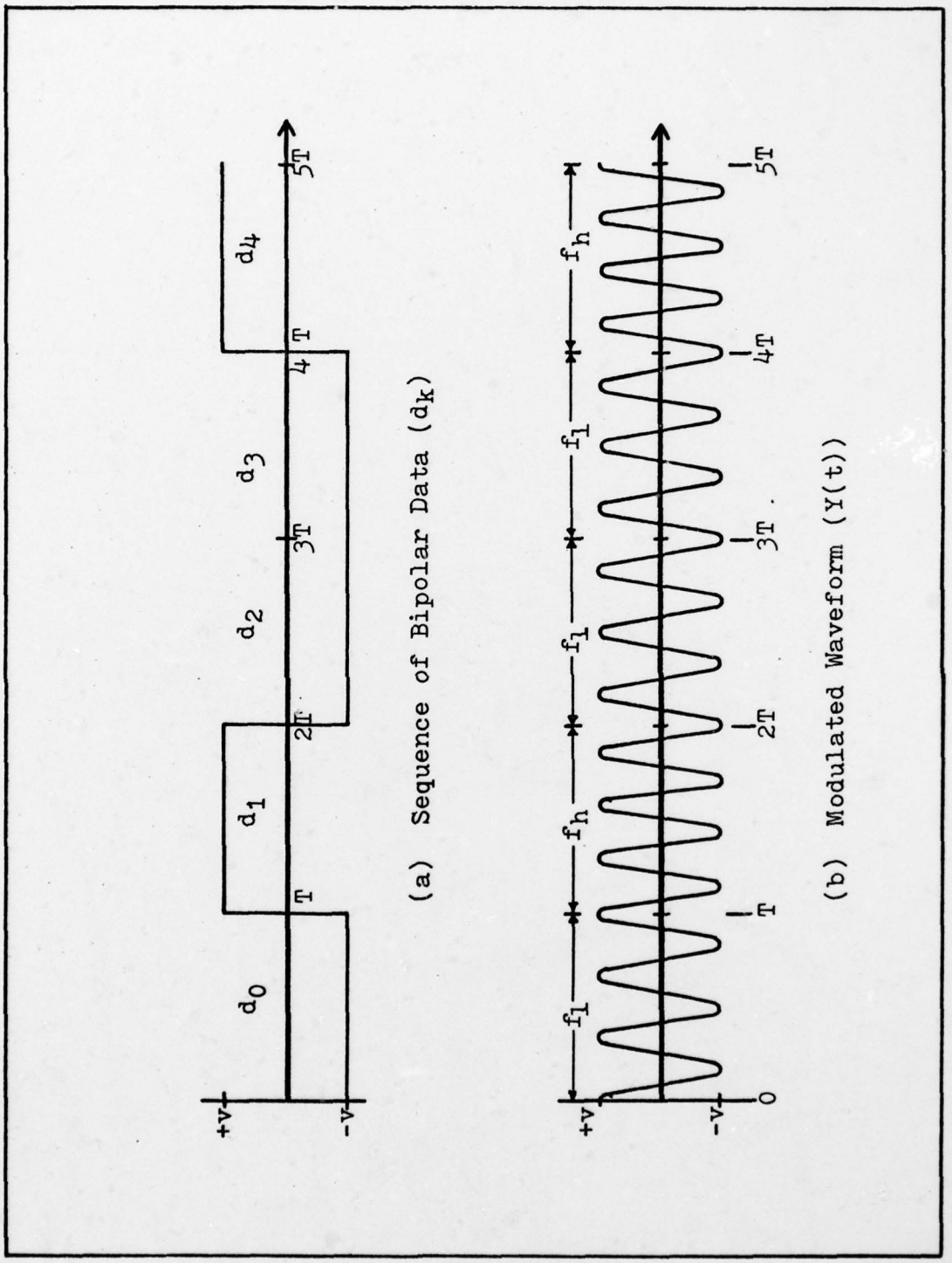


Fig 4. Minimum Shift Keying as a Special Case of Continuous Phase FSK.

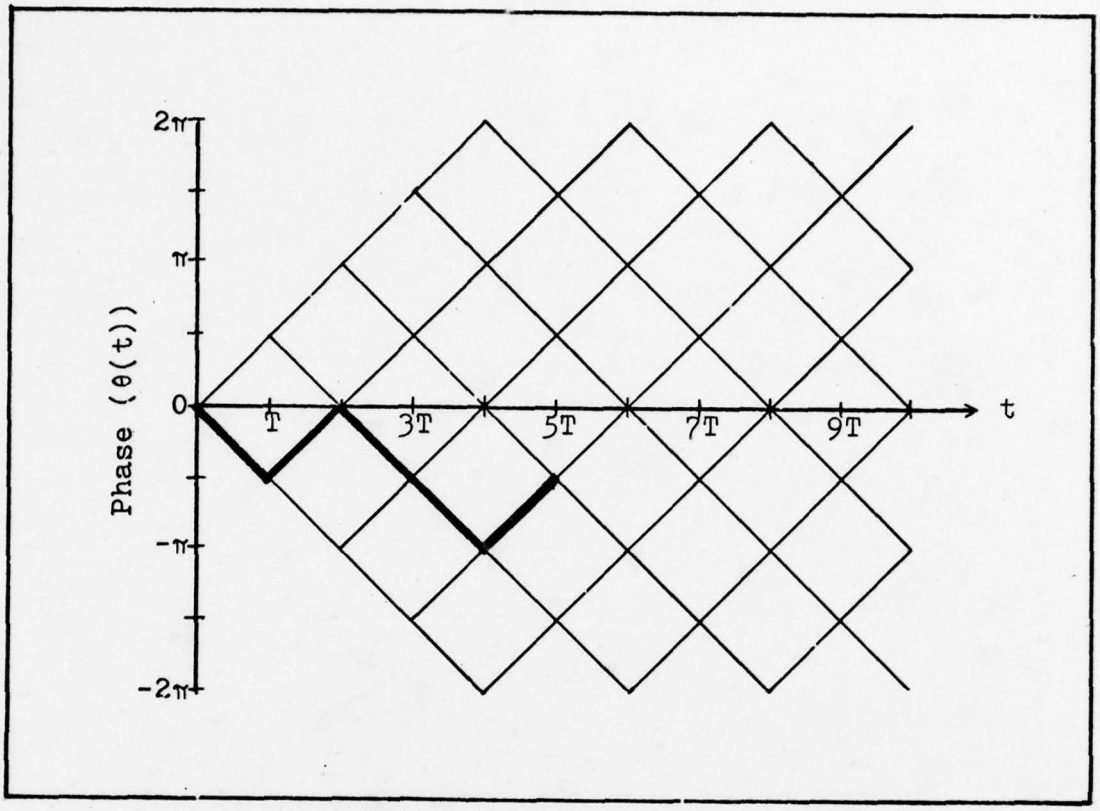


Figure 5. MSK Phase Trellis for Possible Phase Paths, With Phase Changes From the Modulation Carrier Wave of Figure 4 Superimposed

the f_h and f_l tones are orthogonal (correlation = 0) over a signalling interval because the shift in frequency precisely increases or decreases the phase linearly by 90° each data period ($T = \frac{1}{R}$) with respect to the carrier phase. Further, each f_h or f_l tone can occur with positive or negative polarity as a consequence of the relationship between R, f_s and the tone frequencies. The + f_h and - f_h tones are antipodal over a signalling interval, and have correlation equal to - 1. The same is true for the + f_l and - f_l tones (Ref. 14).

The correct relationship between R, f_s and the tone frequencies is easily obtained by choosing a carrier frequency that is an odd multiple of the shift frequency. This is illustrated by the following example:

R = bit rate

R = 21.504 M bits/s (given) (7)

f_s = shift frequency

$f_s = \frac{R}{4}$ = 5.376 MHz (8)

f_c = carrier frequency

$f_c = Nf_s$ where N = odd integer, let N = 13. (9)

f_c = 64.888 MHz

f_h = high tone frequency

$f_h = f_c + f_s$ = 75.264 MHz (10)

f_l = low tone frequency

$f_l = f_c - f_s$ = 64.512 MHz (11)

m = ratio of tone frequency to shift frequency

$$\left.\begin{aligned} m_h &= \frac{f_h}{f_s} = 14 \\ m_l &= \frac{f_l}{f_s} = 12 \end{aligned}\right\} \text{ even multiples as required} \quad (12)$$

using data from the example above, the high tone is "on" for

$$\frac{f_h}{R} = \frac{75.264}{21.504} = 3.5 \text{ cycles} \quad (13)$$

with a data + 1 applied, and the low tone is "on" for

$$\frac{f_l}{R} = \frac{64.512}{21.504} = 3.0 \text{ cycles} \quad (14)$$

with a data - 1 applied, while the carrier has completed

$$\frac{f_c}{R} = \frac{69.888}{21.504} = 3.25 \text{ cycles} \quad (15)$$

Thus, for every T second signalling interval, the phase is linearly increased or decreased 0.25 cycles (± 90°) as required.

Using the binary sequence of data shown in Figure 4(a), the modulated carrier wave shown in Figure 4(b) is generated. During the interval 0 to T seconds, the input bit is data - 1, and a positive polarity low tone is generated. At the end of T seconds, the waveform is at a positive peak, and the next bit is a data + 1, therefore a positive polarity high tone is generated. At the end of 2T seconds, the waveform is at a negative peak and the next bit is a data - 1, therefore a negative polarity low tone is generated. For this illustration, the process continues with switching occurring either at positive or negative peaks of the waveform. For systems that generate sine waves instead of cosine waves, the switching will occur at zero crossings.

Although MSK is a special case of continuous phase two frequency FSK, it can be viewed as sinusoidal shaped OQPSK modulation. This is distinct from the rectangular shaped OQPSK modulation, in that the symbol pulse shapes are a half cycle sinusoid rather than the usual rectangular shape. Sinusoidal shaped OQPSK can be realized mathematically by expressing equation (4) in quadrature notation as

$$Y(t) = \text{Cos}\ (W_c t)\ \text{Cos}\left[\frac{\pi}{2T}\ (t - kT)\ d_k + X_k\right] - \text{Sin}\ (W_c t)\ \text{Sin}\left[\frac{\pi}{2T}\ (t - kT)\ d_k + X_k\right] \qquad (16)$$

Applying the property that $X_k = 0$ or π, modulo 2π, equation (16) reduces to

$$Y(t) = \text{Cos}\ (W_c t)\ \text{Cos}\left[\frac{\pi}{2T}\ (t - kT)\ d_k\right]\ \text{Cos}\ (X_k) - \text{Sin}\ (W_c t)\ \text{Sin}\left[\frac{\pi}{2T}\ (t - kT)\ d_k\right]\ \text{Cos}\ (X_k) \qquad (17)$$

$$(k - 1)\ T \leq t \leq (k + 1)\ T$$

which can be simplified to

$$Y(t) = \text{Cos}\ (X_k)\ C(t)\ \text{Cos}\ (W_c t) - d_k\ \text{Cos}\ (X_k)\ S(t)\ \text{Sin}\ (W_c t)$$

$$kT \leq t \leq (k + 1)\ T \qquad (18)$$

where

$$C(t) = \begin{cases} \text{Cos}\left[\frac{\pi}{2T}\ (t - kT)\right], & kT \leq t \leq (k + 2)\ T \\ 0, & \text{elsewhere} \end{cases}$$

$$S(t) = \begin{cases} \text{Sin}\left[\frac{\pi}{2T}\ (t - kT)\right], & (k - 1)\ T \leq t \leq (k + 1)\ T \\ 0, & \text{elsewhere} \end{cases}$$

In the form of equation (18), MSK is viewed as an inphase and quadrature phase channel employing sinusoidal shaped time-shifted symbol pulses. This representation of MSK is identical to equation (3) for OQPSK, except for the differences in symbol pulse shapes. Sinusoidal shaped OQPSK is shown graphically in Figure 6.

The sinusoidal shape of the symbol pulses result in the phase of the modulated carrier wave transitioning linearly (continuous phase) from one signalling period to another, instead of the abrupt phase changes as in rectangular shaped OQPSK and conventional QPSK. In sinusoidal shaped OQPSK the phase deviation is at a maximum at the end

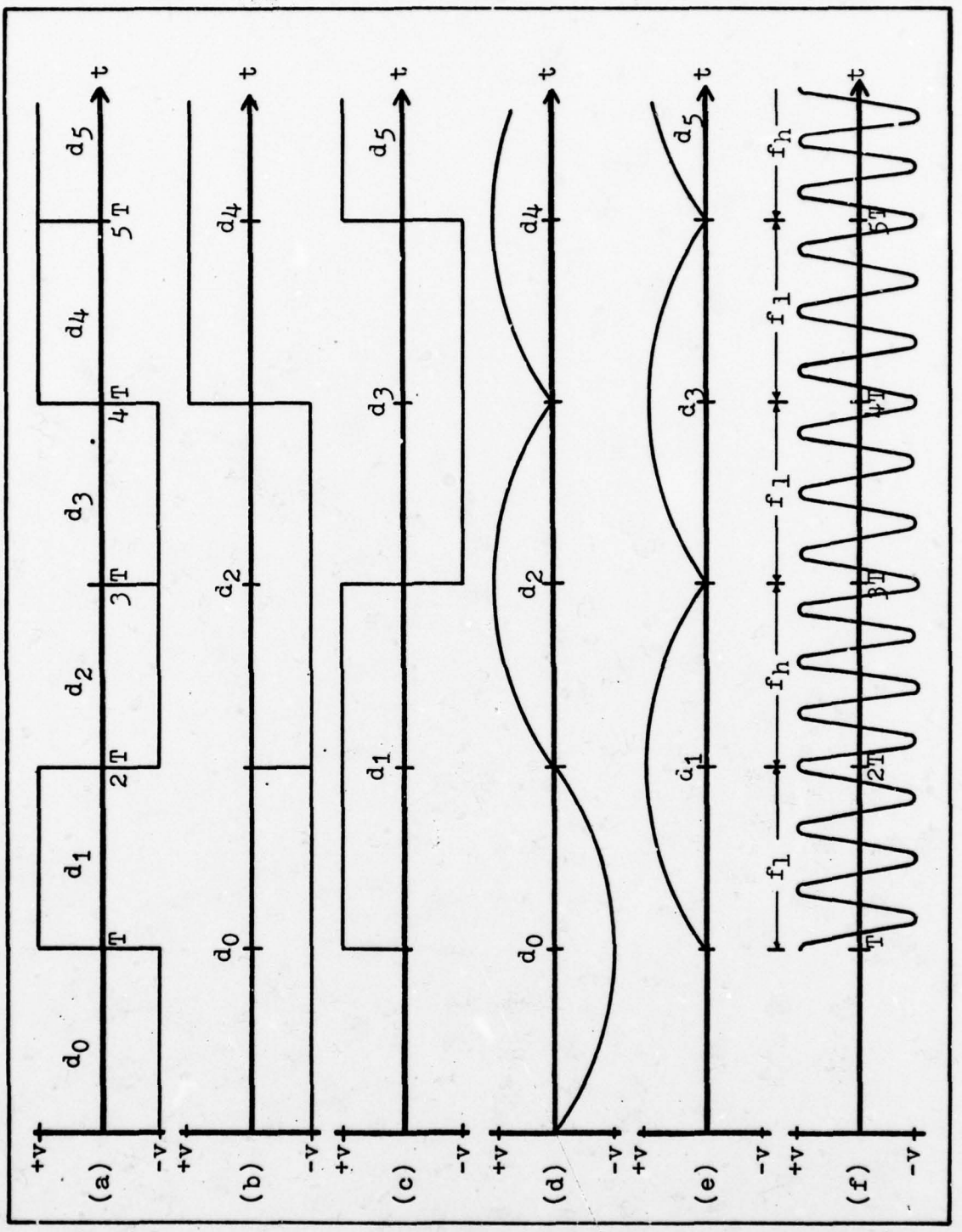


Fig. 6. Example of MSK Waveform as OQPSK With Sinusoidal Shaped Symbol Pulses. (a) Sequence of Bipolar Data (d_k). (b) I Channel Data. (c) Q Channel Data. (d) Sinusoidal Shaped I Channel Data. (e) Sinusoidal Shaped Q Channel Data. (f) Modulated Waveform.

of a signalling interval (see Figure 5), while for rectangular shaped OQPSK, and conventional QPSK, the phase transitions happen instantaneously at the beginning of the signalling interval. It will be shown in Chapter 3, that the continuous phase nature of sinusoidal shaped OQPSK is responsible for the more rapid spectral density roll-off for this modulation technique as compared to rectangular shaped OQPSK or conventional QPSK.

Sinusoidal Frequency Shift Keying (SFSK)

Sinusoidal Frequency Shift Keying (SFSK)[3] is the last constant-envelope modulation techniques with minimum power spectral occupancy to be analyzed. This modulation technique will first be developed as a special case of FSK, then as OQPSK with raise-cosine shaped symbol pulses (raised-cosine shaped OQPSK). For clarity of some passages, the terms SFSK, Sinusoidal Frequency Shift Keying and raised-cosine shaped OQPSK will be used interchangeably.

Sinusoidal Frequency Shift Keying is obtained from FSK by utilizing a raised-cosine (sinusoidal) frequency shift function, instead of the binary frequency shift function of conventional FSK. The frequency shift function in radians per second is expressed as

$$W_{ss}(t) = \frac{d_k \pi}{2T} \left[1 - \text{Cos} \frac{2\pi}{T} (t - kT)\right]$$
$$kT \leq t \leq (k + 1)\, T \qquad (19)$$

[3]Sinusoidal Frequency Shift Keying is sometimes referred to as FM-PSK with raised-cosine signalling (Ref. 12), and as Amoroso's Function (Ref. 3).

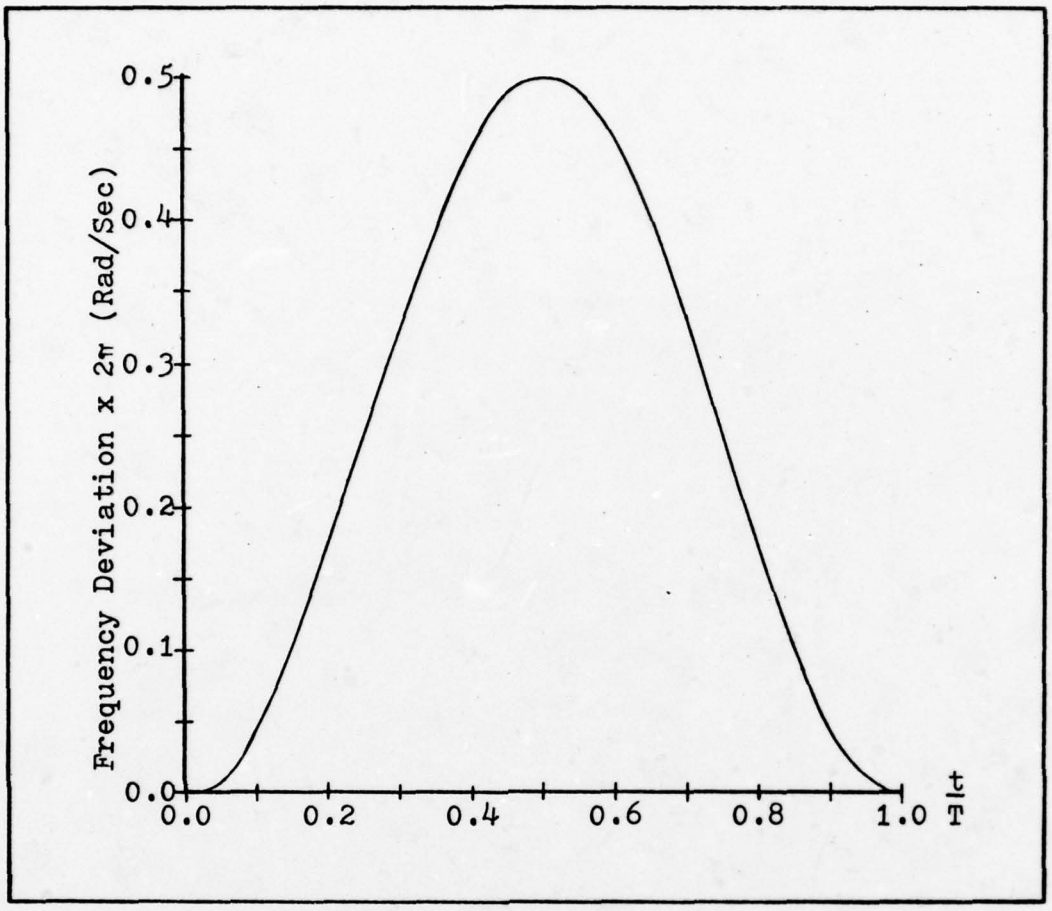


Fig. 7. Raised-Cosine Frequency Shift Function for SFSK.

where $\{d_k = \pm 1\}$ is the input bipolar data stream at the rate $R = \frac{1}{T}$. Equation (19) is plotted in Figure 7, and illustrates that the frequency shift for SFSK is zero at the end points of each T second signalling interval, and in continuous from 0 to T second without any breaks or sharp bends. Maximum frequency deviation occurs when $t = \frac{T}{2}$ and is equal to $\frac{d_k}{2T}$ Hertz. This deviation is twice the frequency shift of MSK, and is equal to the frequency shift of conventional FSK.

Sinusoidal Frequency Shift Keying can be expressed

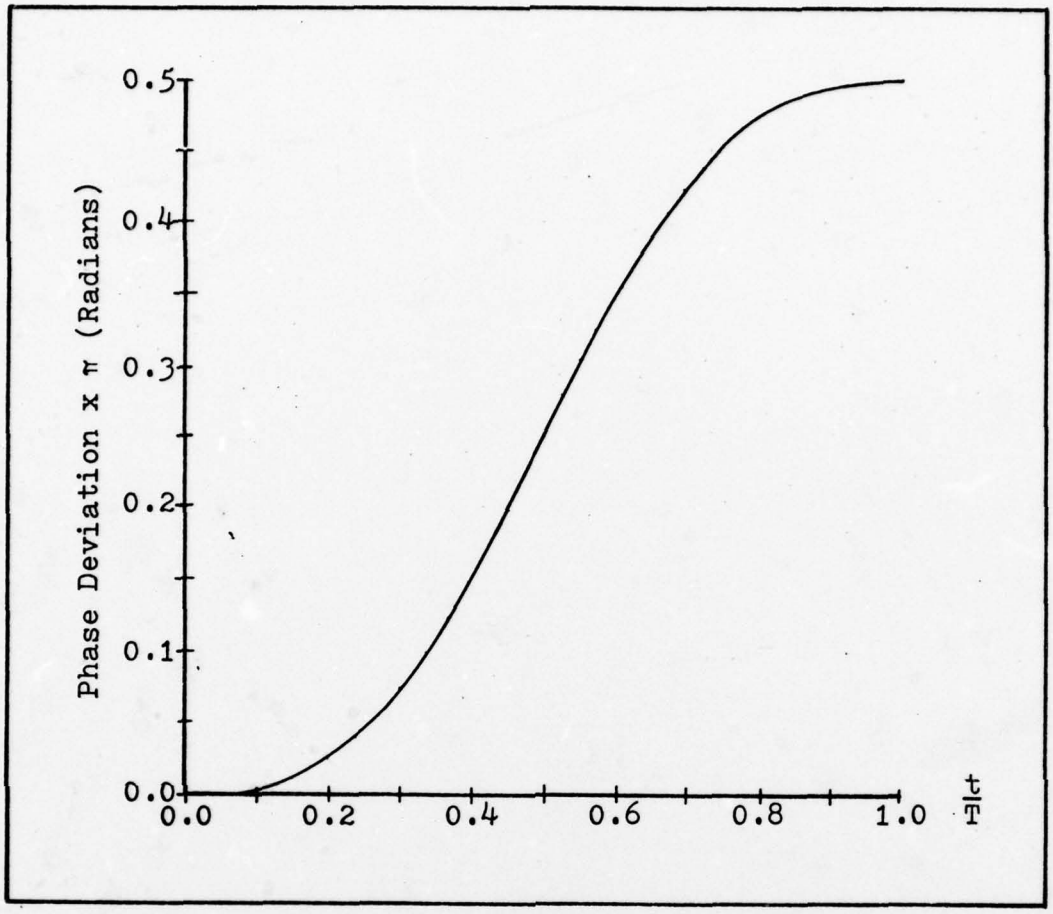


Fig. 8. Phase Deviation Curve for SFSK.

mathematically as a special case of FSK by

$$Y(t) = \text{Cos}\,[W_c t + \theta(t) + X_k], \quad kT \le t \le (k+1)\,T \qquad (20)$$

where $\theta(t)$, the integral of $W_{ss}(t)$, is equal to

$$\theta(t) = \frac{d_k \pi}{2T}\left[(t - kT) - \frac{T}{2\pi}\,\text{Sin}\,\frac{2\pi}{T}\,(t - kT)\right] \qquad (21)$$

and X_k is additive phase which is constant over a data interval. The possible values of X_k are 0 or π, modulo 2π. Equation (21), plotted in Figure 8, illustrates that the phase deviation of SFSK is continuous from 0 to T seconds without any breaks or sharp bends, and that the maximum phase deviation in radians is $\frac{d_k \pi}{2}$ which occurs at t = T

seconds, with respect to the beginning phase. Additionally, because of the zero rate-of-change associated with the beginning and the ending points of the phase deviation curve, the phase changes at the bit transition points are zero. The phase deviation of $\pi/2$ radians (90°) during each T second signalling interval results in adjacent bits being phase orthogonal for bit-to-bit detection. Equations (20) and (21) are plotted in Figure 9, for a given input bipolar data sequence. The convention used is that the modulator transmit an "increasing" frequency deviation for a data + 1, and a "decreasing frequency deviation for a data - 1.

Although SFSK is a special case of FSK, it can be viewed as raised-cosine shaped OQPSK. This is distinct from rectangular shaped or sinusoidal shaped OQPSK, in that the symbol pulse shape is a raised-cosine. The mathematical expression for raised-cosine shaped OQPSK can be realized directly from equation (20) and (21) by following a procedure analogous to the quadrature expansion of equation (4) for MSK. The new expression is

$$Y(t) = \text{Cos}\,(X_k)\, C(t)\, \text{Cos}\,(W_c t) - d_k\, \text{Cos}\,(X_k)\, S(t)\, \text{Sin}\,(W_c t) \qquad kT \le t \le (k+1)\,T \qquad (22)$$

where

$$C(t) = \begin{cases} \text{Cos}\left[\frac{\pi}{2T}\,(t - kT) - \frac{1}{4}\,\text{Sin}\,\frac{2\pi}{T}\,(t - kT)\right], & kT \le t \le (k+2)T \\ 0 & \text{, elsewhere} \end{cases}$$

$$S(t) = \begin{cases} \text{Sin}\left[\frac{\pi}{2T}\,(t - kT) - \frac{1}{4}\,\text{Sin}\,\frac{2\pi}{T}\,(t - kT)\right], & (k-1)T \le t \le (k+1)T \\ 0 & \text{, elsewhere} \end{cases}$$

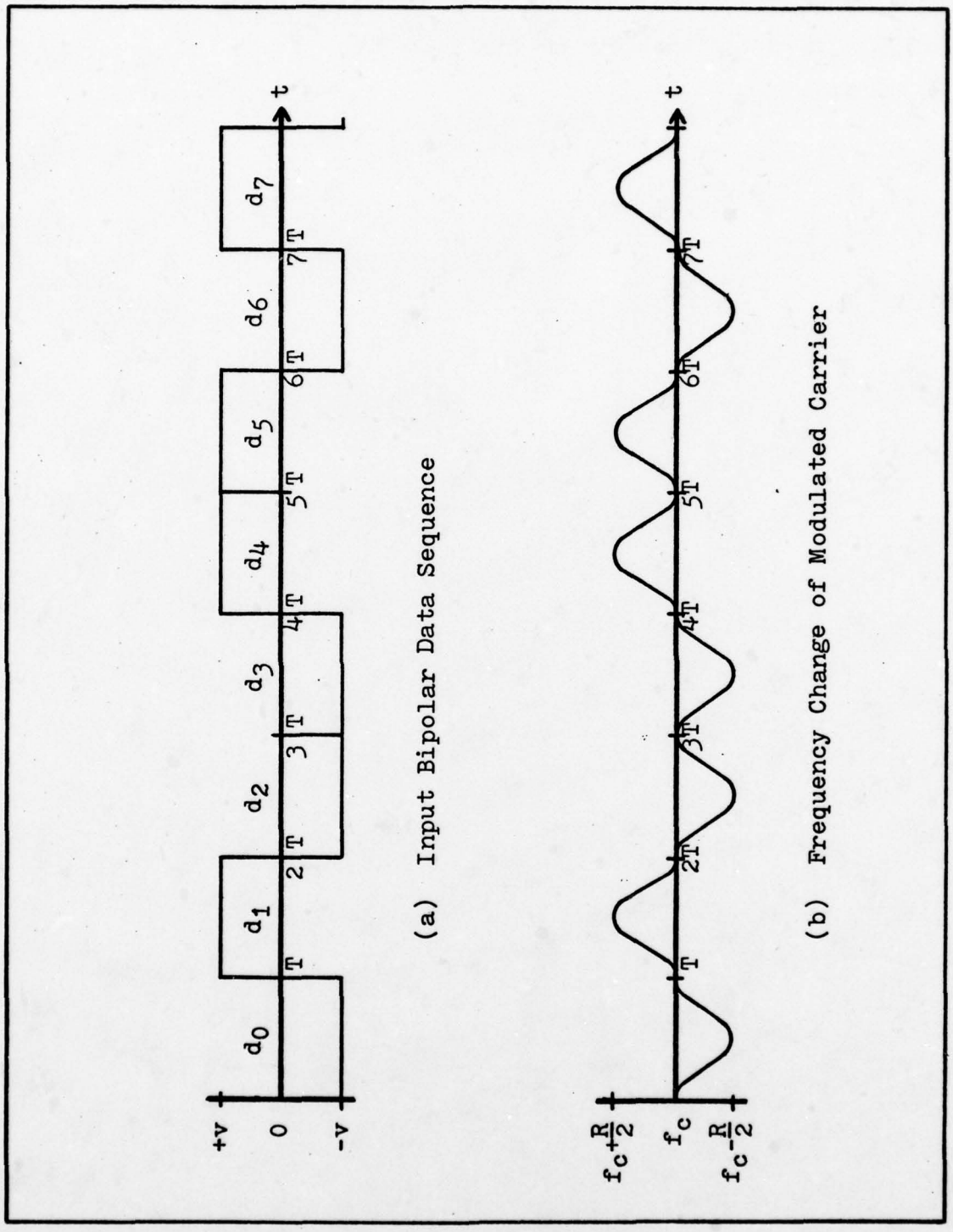


Fig. 9. Sinusoidal Frequency Shift Keying (SFSK) as a Special Case of FSK.

In the form of equation (22) SFSK is viewed as an inphase and quadrature phase channel employing raised-cosine shaped offset, time-shifted symbol pulses. This representation of SFSK is identical to equation (3) for OQPSK, and equation (18) for MSK, except for the differences in symbol pulse shapes. Raised-cosine shaped OQPSK is shown graphically in Figure 10. The raised-cosine shape of the symbol pulse effects both the frequency and phase characteristics of the modulated carrier by insuring that both have a linear transition (continuous frequency and phase) at the bit transition points of the signalling intervals, and a continuous rate-of-change within a signalling interval. It will be shown in Chapter 4, that these properties are responsible for the much more rapid spectral density roll off of SFSK compared to either OQPSK or MSK.

In this chapter the modulation types of OQPSK, MSK and SFSK were introduced and analyzed. Each technique was examined both graphically and mathematically, and a common framework developed. All three types of modulation, when viewed as an inphase and a quadrature phase channel employing offset, time-shifted symbol pulses were shown to be mathematically identical, except for the shape of the symbol pulses. The next chapter will use the common mathematical framework developed in this chapter to determine the autocorrelation, power spectral density and spectral occupancy of the three modulation types.

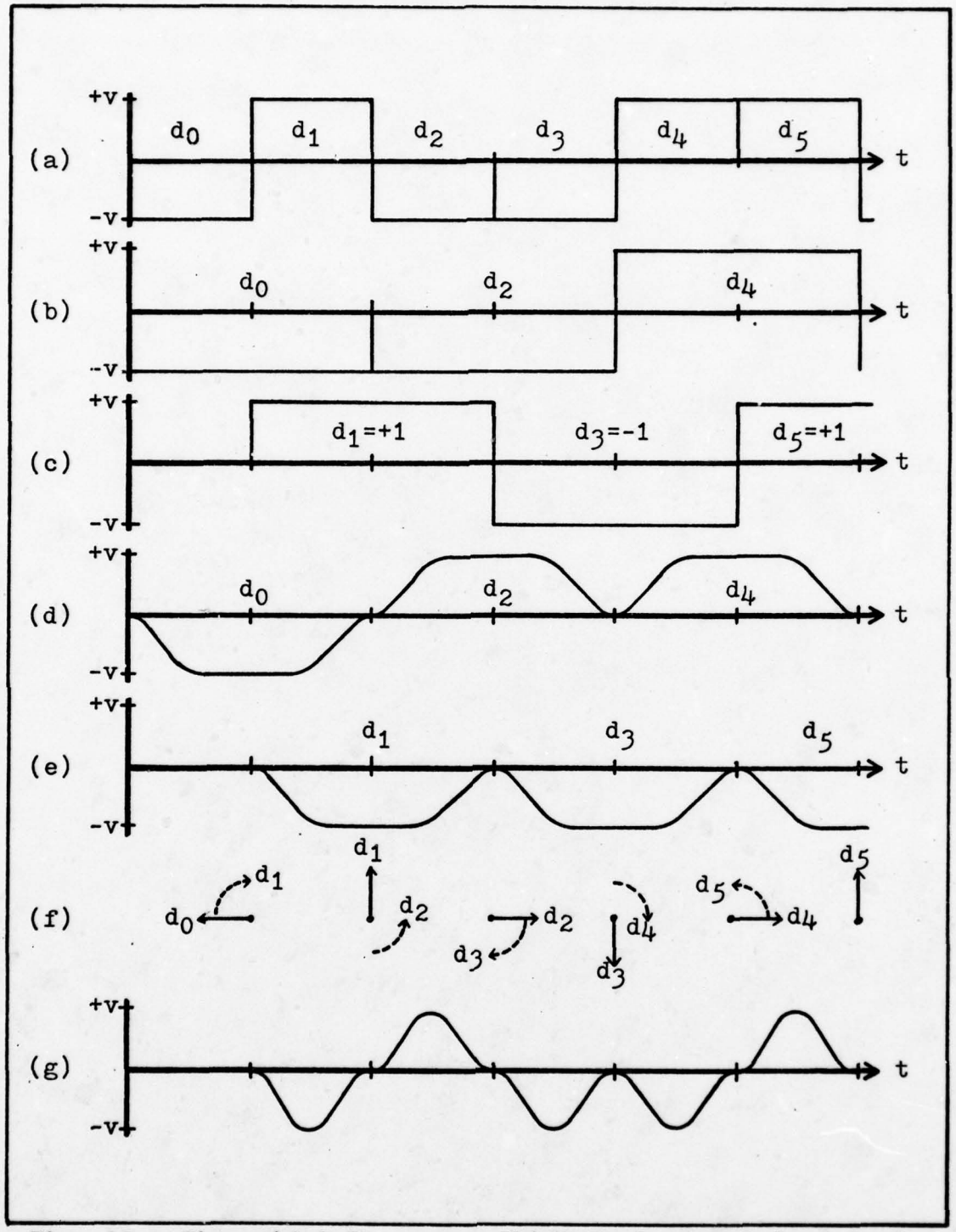


Fig. 10. Sinusoidal Frequency Shift Keying as Raised-Cosine Shaped OQPSK. (a) Sequence of Bipolar Data. (b) I Channel Data. (c) Q Channel Data. (d) I Shaped Channel Data. (e) Q Shaped Channel Data. (f) Phase Deviation of Modulated Carrier. (g) Frequency Deviation of Modulated Carrier.

III Theoretical Spectral Properties

In this chapter, the common mathematical equation developed in Chapter 2 will be expressed in a more straightforward manner, and used to calculate the theoretical spectral properties of OQPSK, MSK and SFSK. The spectral properties as defined here mean the autocorrelation function, power spectral density, spectral occupancy, spectral shape, and roll off characteristics. The term "theoretical" is used to indicate that filters or system nonlinearities have not modified the spectral properties of the modulated waveforms.

Power Spectrum and Autocorrelation Function

The autocorrelation functions and power spectral densities of OQPSK, MSK and SFSK have been evaluated by various authors using a variety of techniques. Simon (Ref. 15) and Gronemeyer and McBride (Ref. 4 and 5) used a first-order Markov approach, Prabhu (Ref. 12) used a matrix approach, while Amoroso (Ref. 10) used a standard Bessel function expansion. In the areas where the papers overlap, the results appear to be in exact agreement.

In this paper, the autocorrelation functions will be computed by using a first-order Markov process model, and the power spectral densities will be computed by taking the Fourier transforms of the autocorrelation functions. This approach will use and duplicate specific steps of references

4, 5, and 15, however, for the greatest part it will expand and clarify the application of the first-order Markov process.

A Markov process model is applicable to these modulation techniques because of the deterministic nature of the output modulated waveforms. The shape (state) of the modulated carrier wave for each of the three modulation techniques is determined by the immediate preceding state of that carrier wave and the input data. The designation "first-order" comes from the dependence of the modulated carrier wave on only the immediate preceding state and not on "m" previous preceding states (Ref. 16:41-3).

The calculation of the autocorrelation function can be simplified by rewriting the common mathematical expression in a more straight-forward manner. In the analysis of Chapter 2, OQPSK, MSK and SFSK were shown to be mathematically identical, except for the shape of the symbol pulses. The common mathematical expression developed was

$$Y(t) = \text{Cos}\,(X_k)\,C(t)\,\text{Cos}\,(W_c t) - d_k\,\text{Cos}\,(X_k)\,S(t)\,\text{Sin}\,(W_c t) \qquad kT \le t \le (k+1)\,T \qquad (23)$$

where C(t) and S(t) represent the symbol pulse sequences defined in equations (3), (18) and (22). This mathematical model contains data terms in which the input bipolar data sequence, d_k, appears encoded as $\text{Cos}\,(X_k)$ and $d_k\,\text{Cos}\,(X_k)$ (data dependent phase terms), and C(t) and S(t) (alternating signal symbol pulse sequences).

An alternate and more straight forward expression is

$$Y(t) = \begin{cases} d_{2k-1}\, C[t-2kT]\, \mathrm{Cos}\,(W_c t) - d_{2k-2}\, S[t-(2k-2)T]\, \mathrm{Sin}(W_c t) \\ \qquad (2k-1)\,T \le t \le 2kT \\ d_{2k-1}\, C[t-2kT]\, \mathrm{Cos}\,(W_c t) - d_{2k}\, S[t-2kT]\, \mathrm{Sin}(W_c t) \\ \qquad 2kT \le t \le (2k+1)\,T \end{cases} \tag{24}$$

where C(t) and S(t) represent the symbol pulse sequences as defined initially. This expression was developed by recognizing that for bit-to-bit independent input data, the sign of successive symbol pulses in either the I or Q channels are random from one 2T second pulse interval to another, and by demultiplixing the input data sequence into odd and even data sequences with the data dependent phase terms encoded. In this form, equation (24) not only mathematically represents the modulation techniques of OQPSK, MSK and SFSK, but the whole class of modulation techniques that employ offset time-shifted symbol pulses in phase quadrature channels (Ref. 5).

This general class of quadrature modulation is completely described by an eight-state transition probability matrix P (Ref. 17:17), the set of initial state probabilities $\{p(i) = \frac{1}{8};\ i = 1, 2\cdots,8\}$, and the set of waveforms associated with each state.

For the sake of convenience, complex envelope notation[4] is used. The state waveform for state i is

[4]Complex envelope notation is expressed mathematically as $Y(t) = \mathrm{Re}\,\{s_i(t)e^{-jw_c t}\}$, and is sometimes referred to as lowpass equivalent notation (Ref. 18:76 and 80).

represented by

$$s_i(t) = s_{ic}(t) + js_{is}(t) \quad i=1,2\cdots,8; \quad kT \le t \le (k+1)T \qquad (25)$$

where $s_{ic}(t)$ is the I channel component, $s_{is}(t)$ is the Q channel component and $\{j = \sqrt{-1}\}$.

The transition probability matrix P consists of the set of probabilities p(i,k), where p(i,k) is defined as the probability of transition from state i to state k at the transition instant, given that the process is currently in state i (Ref. 17:17). For this general class of quadrature modulation there are only two possible values of k for every value of i, hence p(i,k) has the value of 1/2 for these two states and 0 for the other states. The transition matrix P is

$$P = \begin{bmatrix} 0 & 0 & 0 & 0 & \frac{1}{2} & 0 & \frac{1}{2} & 0 \\ 0 & 0 & 0 & 0 & 0 & \frac{1}{2} & 0 & \frac{1}{2} \\ 0 & 0 & 0 & 0 & \frac{1}{2} & 0 & \frac{1}{2} & 0 \\ 0 & 0 & 0 & 0 & 0 & \frac{1}{2} & 0 & \frac{1}{2} \\ \frac{1}{2} & \frac{1}{2} & 0 & 0 & 0 & 0 & 0 & 0 \\ \frac{1}{2} & \frac{1}{2} & 0 & 0 & 0 & 0 & 0 & 0 \\ 0 & 0 & \frac{1}{2} & \frac{1}{2} & 0 & 0 & 0 & 0 \\ 0 & 0 & \frac{1}{2} & \frac{1}{2} & 0 & 0 & 0 & 0 \end{bmatrix} \qquad (26)$$

where

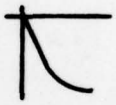
$$s_{1c}(t) = s_{2c}(t) \qquad s_{1s}(t) = s_{3s}(t)$$
$$s_{3c}(t) = s_{4c}(t) \qquad s_{2s}(t) = s_{4s}(t)$$
$$s_{5c}(t) = s_{6c}(t) \qquad s_{5s}(t) = s_{7s}(t)$$
$$s_{7c}(t) = s_{8c}(t) \qquad s_{6s}(t) = s_{8s}(t)$$

The set of waveforms associated with each state is shown in Figures 11, 12 and 13 for OQPSK, MSK and SFSK respectively. Other modulation techniques within this general class of quadrature modulation can be represented in a similar manner.

STATE	I CHANNEL $s_{ic}(t)$	Q CHANNEL $s_{is}(t)$
1	 C(t)	 S(t)
2	 C(t)	 -S(t)
3	 -C(t)	 S(t)
4	 -C(t)	 -S(t)
5	 S(t)	 C(t)
6	 S(t)	 -C(t)
7	 -S(t)	 C(t)
8	 -S(t)	 -C(t)

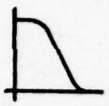
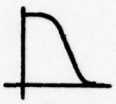
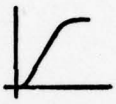
$C(t) = \frac{1}{\sqrt{2}}$ $S(t) = \frac{1}{\sqrt{2}}$

Fig. 11. State Waveforms for Complex Envelope OQPSK.

STATE	I CHANNEL $s_{ic}(t)$	Q CHANNEL $s_{is}(t)$
1	 C(t)	 S(t)
2	 C(t)	 -S(t)
3	 -C(t)	 S(t)
4	 -C(t)	 -S(t)
5	 S(t)	 C(t)
6	 S(t)	 -C(t)
7	 -S(t)	 C(t)
8	 -S(t)	 -C(t)

$C(t)=\text{Cos}[\frac{\pi}{2T}(t-kT)]$ $S(t)=\text{Sin}[\frac{\pi}{2T}(t-kT)]$

Fig. 12. State Waveforms for Complex Envelope MSK.

STATE	I CHANNEL $s_{ic}(t)$	Q CHANNEL $s_{is}(t)$
1	 C(t)	 S(t)
2	 C(t)	 -S(t)
3	 -C(t)	 S(t)
4	 -C(t)	 -S(t)
5	 S(t)	 C(t)
6	 S(t)	 -C(t)
7	 -S(t)	 C(t)
8	 -S(t)	 -C(t)

$$C(t) = \cos\left[\frac{\pi}{2T}(t-kT) - \frac{1}{4}\sin\frac{2\pi}{T}(t-kT)\right]$$

$$S(t) = \sin\left[\frac{\pi}{2T}(t-kT) - \frac{1}{4}\sin\frac{2\pi}{T}(t-kT)\right]$$

Fig. 13. State Waveform for Complex Envelope SFSK.

The general equation for computing the complex envelope autocorrelation function for a random data stream generated by a Markov source (Ref. 5) is

$$R_y(\tau)=R_y(\tau'+mT)$$

$$= \sum_{i=1}^{a} \sum_{k=1}^{a} p(i)p(k|i,m)r_{ik}(T-\tau')+p(k|i,m+1)r_{ki}^*(\tau') \quad (27)$$

for

$$\tau=\tau'+mT\geq 0 \qquad m = \text{integer} \geq 0 \qquad 0\leq\tau'\leq T$$

$$R_y(\tau) = R_y^*(-\tau) \qquad \text{for } \tau < 0$$

where

$$r_{ik}(x) = \frac{1}{T}\int_{kT}^{kT+x} s_i(u)s_k^*(u+T-x)du \qquad 0 \leq x \leq T$$

$s_i(t)$ = waveform of state i

a = number of states = 8

p(i) = probability of state i on $0 \leq t \leq T$

p(k|i,m) = probability of state k on $mT \leq t \leq (m+1)T$ given state i on $0 \leq t \leq T$

= (i,k)th element of the matrix p^m

and the asterisk denotes complex congugate.

Figure 14 shows the complex envelope autocorrelation functions[5] derived by references 4, 5 and 15 from applying equation (27) to the transition probability matrix P, and to the waveforms associated with each state for OQPSK, MSK and SFSK. Note that the autocorrelation functions are zero for

[5]These results were used without mathematical verification because of the agreement between the results derived in references 4, 5, 10, 12, and 15, and the time involved in application of equation (27).

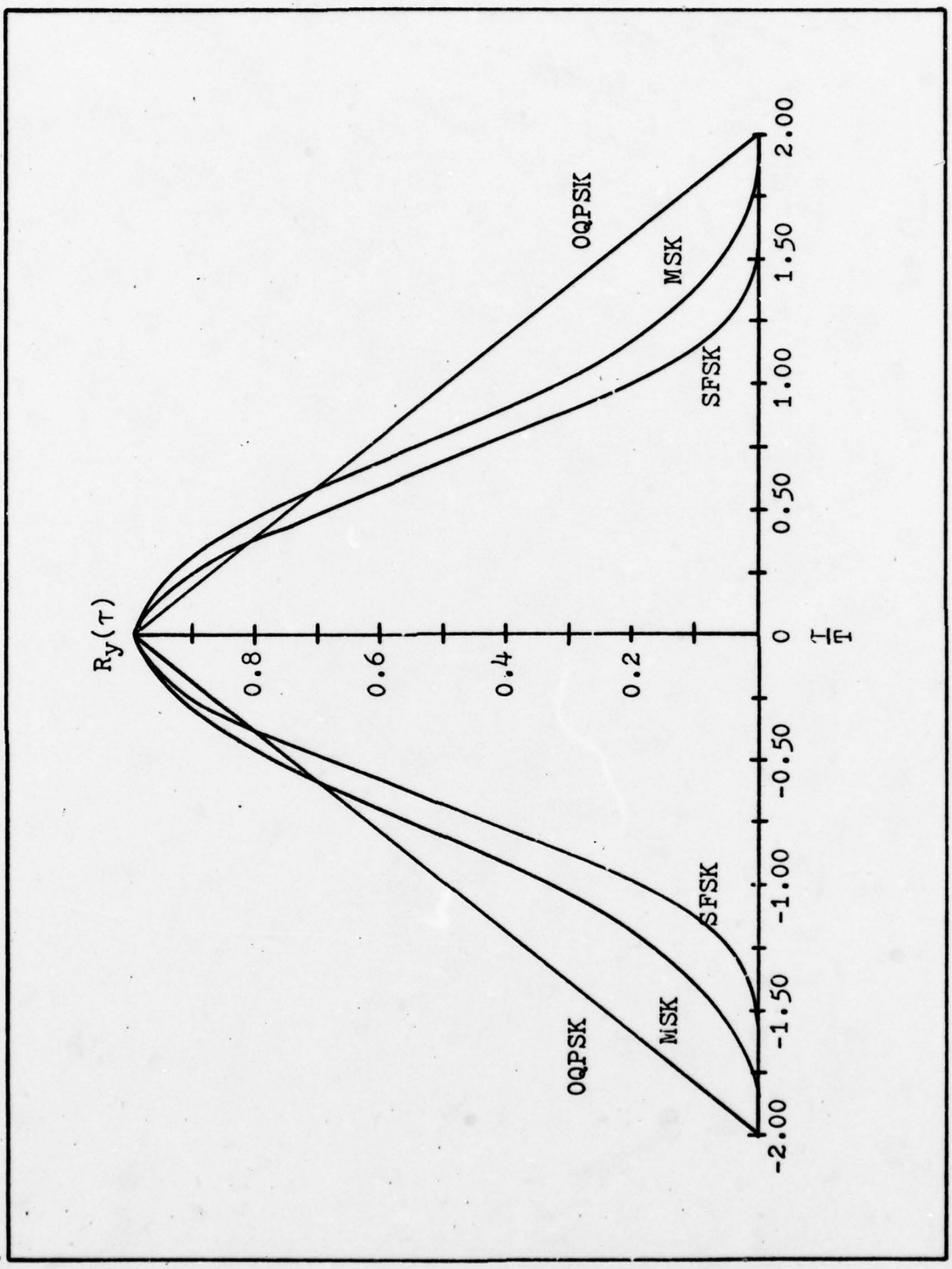


Fig. 14. Comparison of the Normalized Auto-correlation Functions for CQPSK, MSK and SFSK.

all three waveforms for time durations exceeding 2T seconds. The closed form complex envelope autocorrelation functions for OQPSK and MSK are

$$R_{OQPSK}(\tau) = \begin{cases} 1-\frac{|\tau|}{2T}, & \tau \leq 2T \\ 0, & \tau > 2T \end{cases} \quad (28)$$

$$R_{MSK}(\tau) = \begin{cases} \frac{1}{\pi}\{\pi[1-\frac{|\tau|}{2T}]\cos[\frac{\pi|\tau|}{2T}]+\sin[\frac{\pi|\tau|}{2T}]\}, & \tau \leq 2T \\ 0, & \tau > 2T \end{cases} \quad (29)$$

where T is a single data bit duration. For SFSK only numerical results are available. The autocorrelation function for any modulation type within this general class of quadrature modulation can be computed in a similar manner using the transition probability matrix P, given in equation (26), and the waveform associated with each state.

The power spectral density of each modulation technique is the Fourier transform of the corresponding autocorrelation function[6]. For OQPSK the power spectral density is obtained readily through direct application of the Fourier transform definition[7] with integral bounds of (-2T,0) for negative τ, and integral bounds of (0,2T) for positive τ. The power spectral density for MSK is obtained in a similar manner, but only after separating the

---

[6]Alternately, the power spectral density can also be obtained through the use of a first-order Markov approach. This procedure, developed in reference 17:3-17, can be applied to the same transition probability matrix P, and state waveforms derived for the autocorrelation functions.

[7]The Fourier transform used for these calculations is defined by Stein and Jones (Ref. 18:5) as $G(f) = \int_{-\infty}^{\infty} R(\tau)\, e^{-j2\pi f\tau} d\tau$.

autocorrelation function into two parts which are individually transformed. The complex envelope power spectral densities for OQPSK and MSK are

$$G_{OQPSK}(f) = 2PcT \left[\frac{\text{Sin } 2\pi fT}{2\pi fT}\right]^2 \tag{30}$$

$$G_{MSK}\ (f) = \frac{8PcT\ (1 + \text{Cos } 4\pi fT)}{\pi^2(1 - 16T^2f^2)^2} \tag{31}$$

where

f = frequency offset from carrier

Pc = power in modulator waveform

T = single data bit duration

A closed form expression for the power spectral density of SFSK is not currently available, however, its integral definition (Ref. 10) can be expressed as

$$G_{SFSK}(f) = 2\int_0^{T/2} \{\text{Cos } 2\pi fT \text{ Cos } [\Delta\phi(t)] + \text{Cos } 2\pi f(T-t) \text{ Sin } [\Delta\phi(t)]\}\, dt \tag{32}$$

where

$$\Delta\phi(t) = \frac{\pi t}{2T} - \frac{1}{4} \text{Sin } \frac{2\pi t}{T}$$

Equations (30) and (31), and a numerically derived power spectral density for SFSK (Ref. 15) are plotted in Figure 15 as a function of f normalized to the input data rate $R = \frac{1}{T}$.

The amplitude of the power spectral densities for OQPSK, MSK and SFSK roll off at rates proportional to $(f/R)^{-2}$, $(f/R)^{-4}$, and $(f/R)^{-8}$ respectively for large values of f/R. The main lobes have first nulls falling at f/R = 0.50, 0.75 and 0.86 respectively.

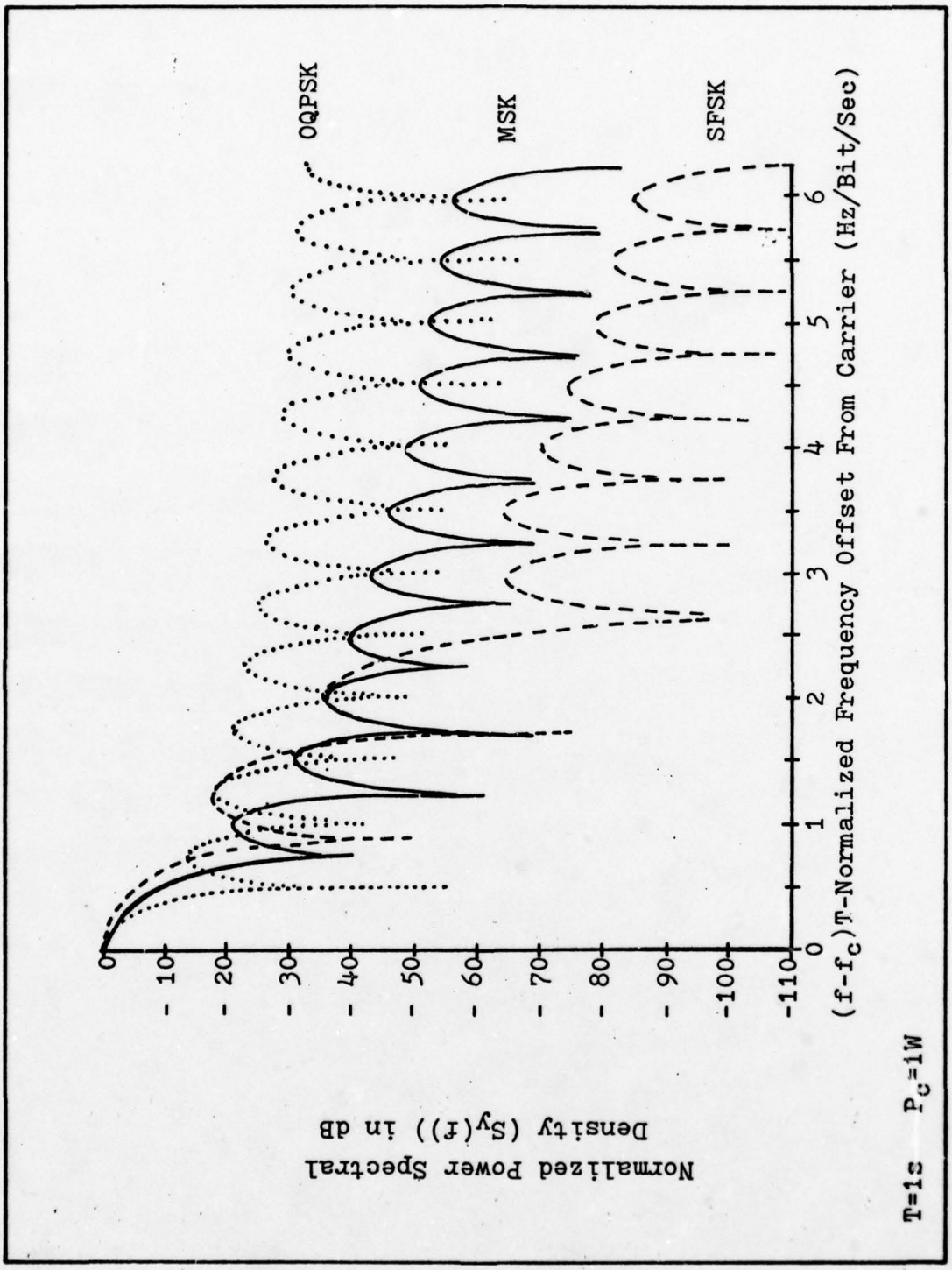


Fig. 15. Comparison of Power Spectral Densities for OQPSK, MSK and SFSK.

Not shown by Figure 15 or equation (30) is that the power spectral density of OQPSK is identical to the power spectrum of QPSK (Ref. 19). Additionally, the power spectrum of PSK is identical to QPSK, except that the data rate R for PSK is only one half that of QPSK. Thus, for the same input data rate, the power spectral density of QPSK is one half the bandwidth of PSK.

Spectral Occupancy

The spectral occupancy of OQPSK, MSK and SFSK will be analyzed in this paper by two distinct methods. First, the out-of-band power of each modulation technique will be analyzed as a function of the bandwidth. Second, for each modulation technique, the mean-square crosstalk $E(C^2)$ between two adjacent channels whose center frequencies are separated by Δ_f Hertz will be computed.

Out-of-Band Power. A measure of the total out-of-band power of any modulated waveform is provided by the fractional out-of-band power ratio, P_{ob} (Ref. 5). This ratio is defined as the fraction of the total power in the spectrum which does not pass through a rectangular filter of frequency interval (-B,B). The transfer function of the filter is nonzero only in the (-B,B) frequency interval, and equal to zero elsewhere. The fractional out-of-band power is expressed as

$$P_{ob} = 1 - \frac{\int_{-B}^{B} S(f)\, df}{\int_{-\infty}^{\infty} S(f)\, df} \qquad (33)$$

Equation (33) evaluated for the power spectral densities of PSK, OQPSK, MSK and SFSK is plotted in Figure 16 as a function of B normalized to the binary data rate $R = \frac{1}{T}$.

Prabhu (Ref. 12) showed that for this general class of quadrature modulation a finite limit in the compactness of a power spectrum exists, regardless of the input symbol pulse shape. This limit in spectral compactness is plotted in Figure 16 as a lower bound on the minimum fractional out-of-band power possible.

Figure 16 indicates that for system bandwidth exceeding about 3.0 f/R, SFSK has lower fractional out-of-band power than MSK or OQPSK, while for system bandwidths from about 3.0 to 1.5 f/R, MSK has the lowest fractional out-of-band power. However, as system bandwidth is decreased below 1.0 f/R, a point is reached where OQPSK has fractional out-of-band power lower than MSK or SFSK. As system bandwidth is increased toward infinity, the fractional out-of-band power of the three systems converge and become equal.

The two sided bandwidth requirement for OQPSK, MSK, SFSK and the lower bound are summarized in Table I for out-of-band power ratio values of 0.1, 0.01 and 0.001. An out-of-band ratio of 0.1 indicated 90 percent of the power is contained within the frequency band (-B,B) while ratios of 0.01 and 0.001 indicate that 99 percent and 99.9 percent respectively, of the total power is contained within the band. Note that the two sided bandwidth requirement for

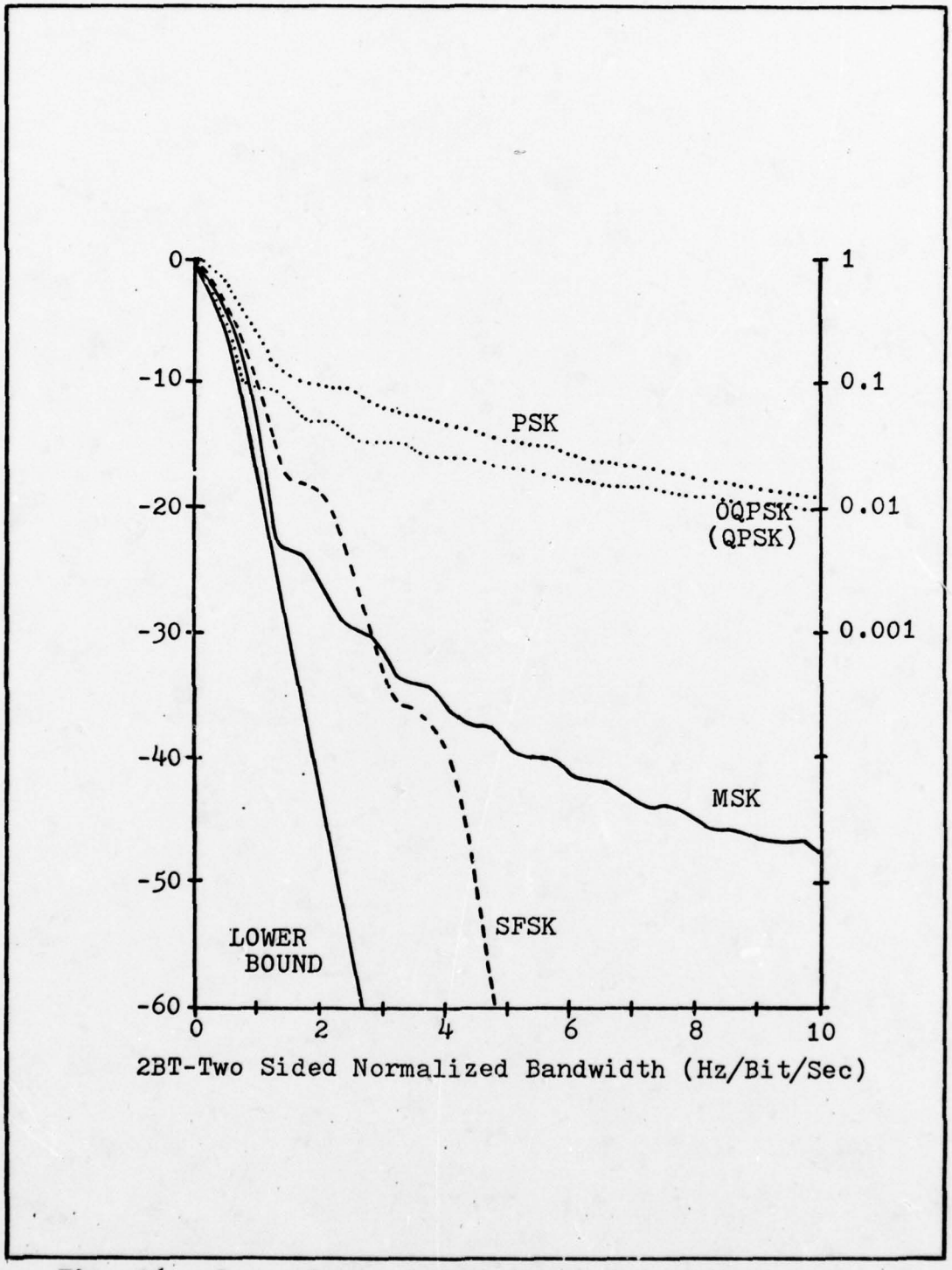


Fig. 16. Comparison of Fractional Out-of-Band Power for PSK, OQPSK, MSK, SFSK and the Lower Bound for Any Symbol Pulse Shape.

TABLE I

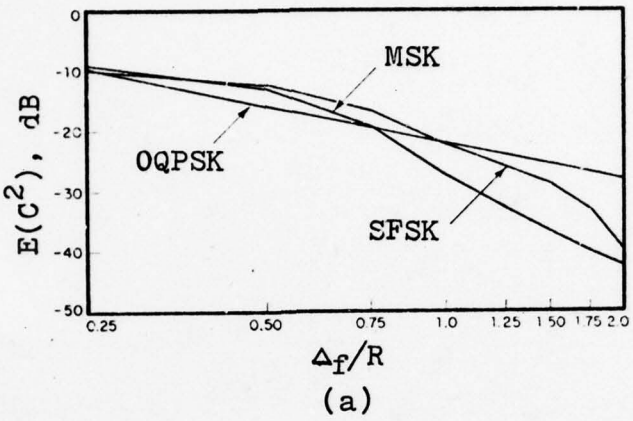
Summary of Two Sided

Bandwidth Requirements

Pob	Lower Bound	OQPSK	MSK	SFSK
0.1	0.68	0.77	0.77	0.93
0.01	1.12	8.00	1.17	2.20
0.001	1.52	≈27	2.58	2.87

MSK is very close to the lower bound for out-of-band power ratio values between 1 and 0.01, and at 0.01, the necessary bandwidth is only about 5 percent higher than the lower bound. Note also that the bandwidth occupancy of MSK is smaller than SFSK for out-of-band power ratios less than or equal to 0.001.

Mean-Square Crosstalk. An alternate measure of spectral occupancy is the average mean-square crosstalk $E(C^2)$ between two adjacent channels of a particular modulation type with center frequencies separated by Δ_f/R. Calculations of this nature for OQPSK, MSK and SFSK have been made by Kalet (Ref. 3) with the results shown in Figure 17(a) and 17(b). These figures, similar to Figure 16 for out-of-band power, show that crossover points exist in performance between these modulation types. Figures 17(a) and 17(b) indicate that for values of Δ_f/R greater than about 2.3, two SFSK



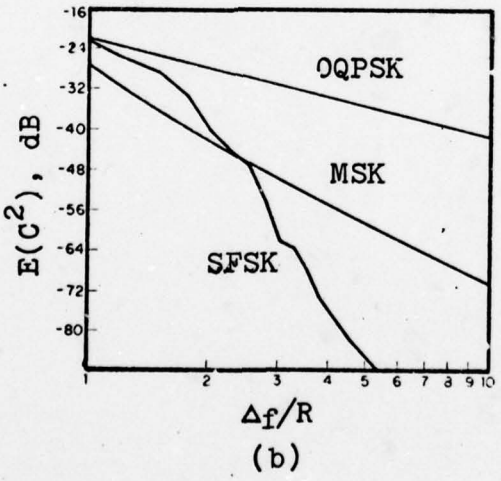


Fig. 17. Mean-Square Crosstalk $E(C^2)$ Between Two Adjacent Channels of Like Modulation for OQPSK, MSK and SFSK. The Center Frequency Separation Between the Two Adjacent Channels is Δ_f/R.

channels have less mean-square crosstalk than two channels of MSK or OQPSK, while for values of Δ_f/R between about 0.75 and 2.3 two MSK channels have the lowest mean-square crosstalk. However, for values of Δ_f/R less than 0.75, two OQPSK channels have the lowest mean-square crosstalk.

Spectral Shape

Spectral shape is a term used to denote the physical shape of the power spectral density. Properties of the physical shape such as the width of the main lobe, magnitude of particular frequencies and roll off characteristics are needed for determining spectral occupancy and out-of-band emission levels. These characteristics can be determined or predicted to a large extent by observing the shape of the autocorrelation function.

The power spectral density, as indicated earlier is related to the autocorrelation function by

$$G(f) = \int_{-\infty}^{\infty} R(\tau)e^{-j2\pi f\tau}\, d\tau \qquad (34)$$

The mathematical relationship between the shape of the autocorrelation function and the power spectral density can be developed by combining the differentiation property of the Fourier transform (Ref. 7:36)

$$\frac{d^n R(\tau)}{d\tau^n} \longleftrightarrow (j2\pi f)^n\, G(f) \qquad (35)$$

with equation (34) where "n" equals the order of the derivative. The resulting equation is

$$(j2\pi f)^n\, G(f) = \int_{-\infty}^{\infty} \frac{d^n}{d\tau^n} R(\tau)e^{-j2\pi f\tau}\, d\tau \qquad (36)$$

Taking the absolute value of both sides gives

$$\left| (j2\pi f)^n G(f) \right| = \left| \int_{-\infty}^{\infty} \frac{d^n}{d\tau^n} R(\tau) e^{-j2\pi f\tau} \right| d\tau \qquad (37)$$

which reduces by Schwarz's inequality to

$$(2\pi f)^n \left| G(f) \right| \leq \int_{-\infty}^{\infty} \left| \frac{d^n}{d\tau^n} R(\tau) \right| \left| e^{-j2\pi f\tau} \right| d\tau \qquad (38)$$

This equation can be further simplified by dividing both sides of the inequality by $(2\pi f)^n$, and noting that $R(\tau)$ is time limited $(-2T,2T)$, and $\left|\exp(-j2\pi f\tau)\right| = 1$. The desired relationship is

$$\left| G(f) \right| \leq \frac{1}{(2\pi f)^n} \int_{-2T}^{2T} \left| \frac{d^n}{d\tau^n} R(\tau) \right| d\tau \qquad (39)$$

Equation (39) shows that the magnitude and roll off of $G(f)$ is bounded by the derivatives of the autocorrelation function. Mason and Zimmermann (Ref. 20:237) show graphically that the magnitude and width of the main lobe are bounded when $n = 0$, and that the magnitude and slope of the tails are bounded when $n = 1$ and 2.

It can be shown by further elaboration of equation (39) that for time limited functions, the roll off characteristics of $G(f)$ are dependent on the behavior of $R(\tau)$ near the end points $\tau = \pm 2T$ of the interval $(-2T,2T)$. At the end points, the derivatives are defined as interior limits:

$$\frac{d^n}{d\tau^n} R(-\tau) = \lim_{\epsilon \to 0} \frac{d^n}{d\tau^n} R(-\tau+\epsilon) \qquad (40)$$

$$\frac{d^n}{d\tau^n} R(\tau) = \lim_{\epsilon \to 0} \frac{d^n}{d\tau^n} R(\tau-\epsilon) \qquad (41)$$

where ϵ, the incremental distance along the τ axis is greater than zero, but approaching zero.

Since $R(\tau) = 0$ for $|\tau| > 2T$, if the n order derivative

$$\frac{d^n}{d\tau^n} R(\pm 2T) \neq 0 \tag{44}$$

then an impulse exists at $\tau \pm 2T$ for that derivative. Therefore, for a rapid roll off characteristic of $G(f)$, $R(\tau)$ must have a high order of derivatives at the end points ($\tau = \pm 2T$) equal to zero (high order of tangency with the τ axis). This relationship is stated more definitively by Papoulis (Ref. 21:188) as[8]

$$\frac{d^k}{d\tau^k} R(-\tau) = 0, \quad \frac{d^k}{d\tau^k} R(\tau) = 0, \quad k = 0,1,\ldots,n-1$$

$$G(W) = 0\left(\frac{1}{W^{n+1}}\right) \qquad W \to \infty \tag{45}$$

where $R(\tau)$ has bounded derivatives of order up to n for every $|\tau| < 2T$, and at the end points $\tau = \pm 2T$.

This characteristic is illustrated by the autocorrelation functions, the first and second derivatives of the autocorrelation functions, and the power spectral densities of OQPSK, MSK and SFSK shown in Figures 14, 15, 18 and 19. The OQPSK autocorrelation function is continuous at $\tau = \pm 2T$, but its first derivative is discontinuous at this point; hence, $G_{OQPSK}(W) = 0(1/W^2)$. The MSK autocorrelation function and its first and second derivatives are continuous at $\tau = \pm 2T$, but the third derivative is discontinuous at this point; hence, $G_{MSK}(W) = 0(1/W^4)$.

[8]The notation $0\left(\frac{1}{W^n}\right)$ indicates that the value of the function is approaching zero at the rate $\frac{1}{W^n}$ as W approaches ∞ (Ref. 18:230).

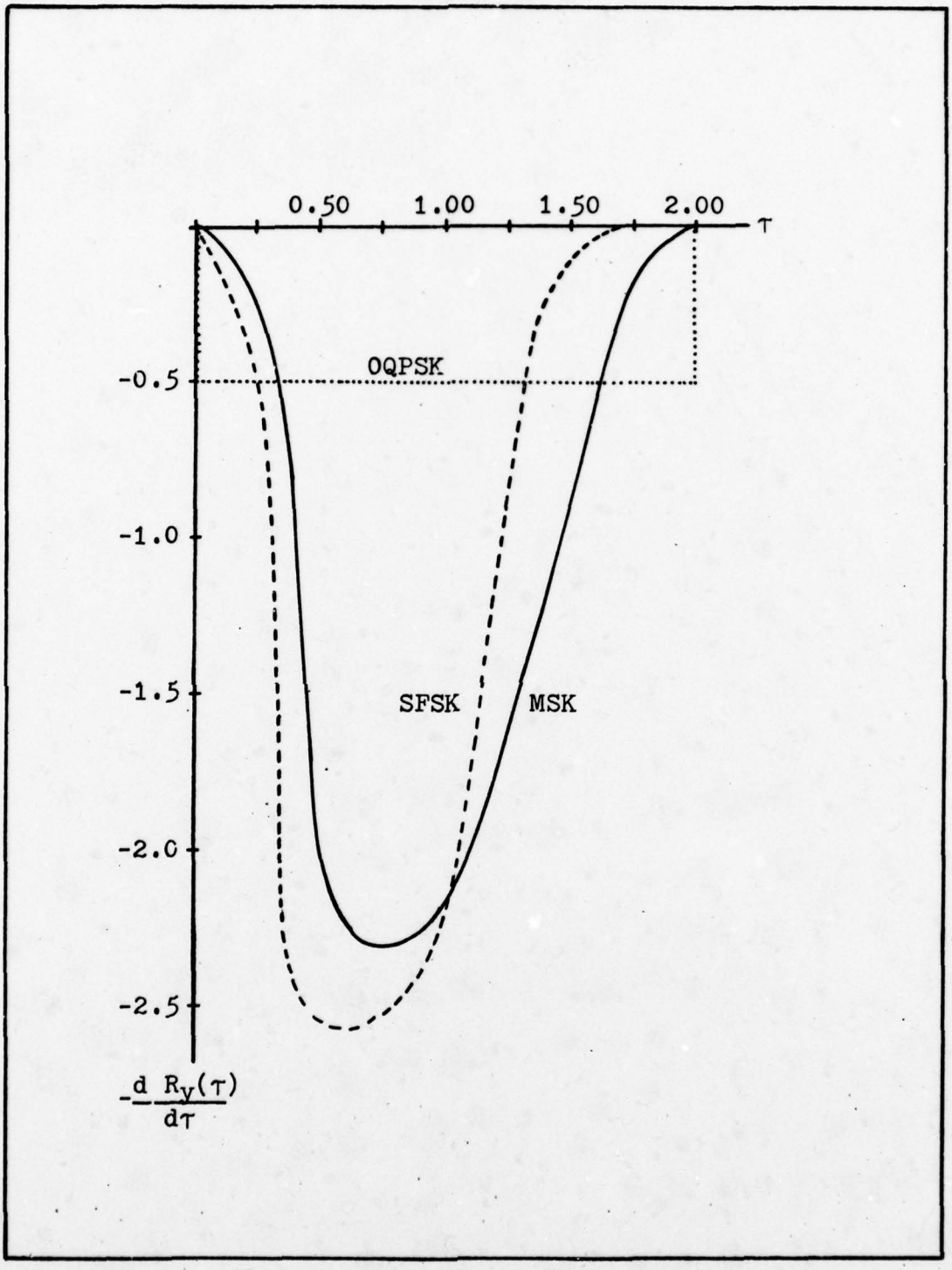


Fig. 18. First Derivative of Autocorrelation Function for OQPSK, MSK and SFSK (Positive τ Only).

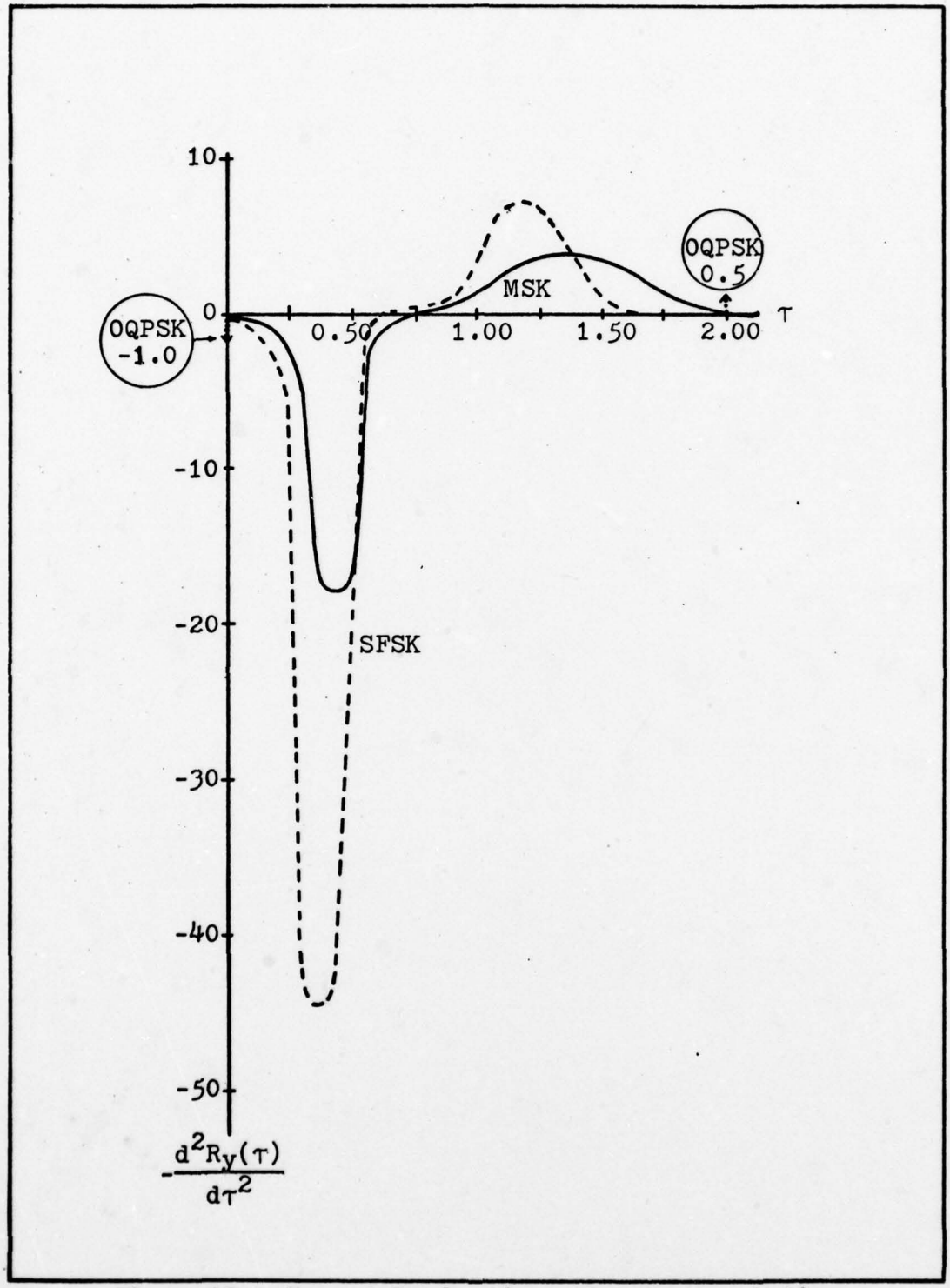


Fig. 19. Second Derivative of Autocorrelation Functions for OQPSK, MSK and SFSK (Positive τ Only).

Finally, the SFSK autocorrelation function and its first six derivatives are continuous at $\tau = \pm 2T$, but the seventh derivative is discontinuous at this point; hence $G_{SFSK}(W) = O(1/W^8)$.

Two additional observations can be obtained from this relationship. First the width of the main lobe of the power spectral density is directly related to the order of tangency of the autocorrelation function (see Figures 14 and 15). This action is the result of compacting more of the spectral power into a smaller bandwidth as the amplitude of the side lobes are reduced. Second, the maximum value of the slope of the autocorrelation function is directly related to its order of tangency (see Figures 14 and 18).

This characteristic can be illustrated mathematically by a Taylor series expansion (Ref. 22:576) of $R(\tau)$ about the end points. At $\tau \leq 2T$, but near 2T, $R(\tau)$ has the following expansion:

$$R(\tau) = R(2T)+R'(2T)(\tau-2T)+\frac{R''(2T)}{2!}(\tau-2T)^2+\frac{R'''(2T)}{3!}(\tau-2T)^3+\ldots$$
$$+\frac{R^{(n)}(2T)}{n!}(\tau-2T)^n+\ldots \qquad (44)$$

The term $R^{(n)}(2T)$ denotes the order of the derivative of the autocorrelation function, while $(\tau-2T)^n$ is an incremental distance term raised to the power n. For an order of tangency of n, all derivatives up to and including n are zero, with

$$R(\tau) = R(2T)+\frac{R^{(n+1)}(2T)}{(n+1)!}(\tau-2T)^{n+1}+\frac{R^{(n+2)}(2T)}{(n+2)!}(\tau-2T)^{n+2}+\ldots \qquad (45)$$

representing the curve. Since the incremental distance term $(\tau - 2T) \leq 1$, the power of its exponent determines to a great degree how far τ must decrease from 2T before $R(\tau)$ can increase to a predetermined value δ. The further τ must decrease from 2T before $R(\tau)$ reaches the value δ, the greater the resulting slope of $R(\tau)$ must be to reach the value of 1 at $\tau = 0$. Thus, the higher the order of tangency, the larger the exponent of $(\tau - 2T)$ and the larger the absolute value of the slope.

The relationship existing between the shape of the autocorrelation function and the shape of the power spectral density also exists to a large degree between the shape of the modulating symbol pulse and the shape of the power spectral density. This is because the Fourier transform of a signal gives the amplitude of the frequency components, while the Fourier transform of its autocorrelation function gives the power spectral density. Thus, the order of tangency of the symbol pulse shape can be used to predict, with some accuracy, the shape of the power spectrum.

This relationship can be illustrated by considering the shape of the symbol pulses of OQPSK, MSK and SFSK given in equations (3), (18) and (22) respectively. The sinusoidal symbol pulse of MSK has a higher order of tangency than that of OQPSK; hence, it has a more compressed power spectrum and a faster roll off characteristic. The raised-cosine symbol pulse of SFSK has a higher order of tangency than OQPSK or MSK; hence, it has a more compressed power spectrum and

faster roll off than either. Similar results could also be observed for PSK and QPSK in the papers by Prabhu (Refs. 12 and 23) and Greenstein (Ref. 24) as the pulse shape of a signalling waveform was varied.

An interesting practical application of this principle can be observed in a paper by Anderson (Ref. 2). Anderson described obtaining a 30dB reduction in PSK sideband power by filtering the input binary data sequence. The filtering process smoothed the corners of the binary data pulses (rectangular symbol pulses), thus increasing the order of tangency of the symbol pulse with the t axis, and improving as predicted the roll off characteristics of the power spectrum.

In this chapter the theoretical spectral properties of OQPSK, MSK and SFSK were calculated. Additionally, the relationships between the shape of the autocorrelation function and the symbol pulse to the shape of the power spectral density were analyzed and developed. It was shown that the width of the main lobe of the power spectrum and the spectral roll off are directly related to the tangency (smoothness) of the symbol pulse and the autocorrelation function. The next chapter will evaluate the performance of OQPSK, MSK and SFSK in practical situations with filters, limiters and nonlinear conditions.

IV Practical Spectral Properties

In this chapter the performance of OQPSK, MSK and SFSK will be evaluated using practical channel conditions of filters, limiters and nonlinear devices. This will be accomplished first by analyzing the characteristics of filters and limiters as individual items, then as applied to OQPSK, MSK and SFSK. Next, the simulated performance of OQPSK and MSK will be given and compared using probability of error as the figure of merit.

Practical System Devices

In this section the characteristics of filters and limiters as individual components will be analyzed.

Filter Characteristics. Theoretically, an ideal filter passes all frequencies within its passband, without distorting the amplitude or phase of those frequencies, while rejecting the frequencies outside of the passband. Filtering a rectangular data pulse sequence with an ideal filter whose bandwidth is on the order of the data rate should result in only the rounding of the edges of each pulse (removal of the high frequencies). However, practical filters have phase distortion, particularly at the edges of the passband, which causes each pulse within the data sequence to be delayed and stretched in time. Thus, the pulses overlap and interfere with each other. This smearing of the pulses is a phenomenon known as intersymbol interference.

Filtering a modulated carrier wave with a practical filter whose bandwidth is on the order of the signalling rate results in the output symbol pulses (symbol pulses of the modulated carrier wave) experiencing the same changes as the rectangular data pulses described above. Thus, the output symbol pulses are rounded, delayed and stretched, with overlapping and interference. The extent of the smearing depends upon the rate-of-change in amplitude and phase the output symbol pulses possess. This smearing may either reinforce or oppose accurate detection of the output symbol pulses, however, on the average, the error performance is degraded.

Limiter Characteristics. The limiting process is a technique to normalize the envelope of a signal. The degree of normalization is a function of the type of limiting used. The two most common types of limiters (Ref. 20) are shown in Figure 20. In this form, $Y(t)$ indicates the output envelope, $X(t)$ the input envelope, Y_m the maximum amplitude of the output envelope, and X_m the hard limiting point of the soft limiting curve. As illustrated, hard limiting performs almost a complete normalization of the signal, while soft limiting only a partial normalization.

For digital transmission with constant envelope, as assumed in the introduction to this paper, hard limiting is most often used. The output-to-input relationship for a hard limiter using complex envelope notation (Refs. 5 and 9)

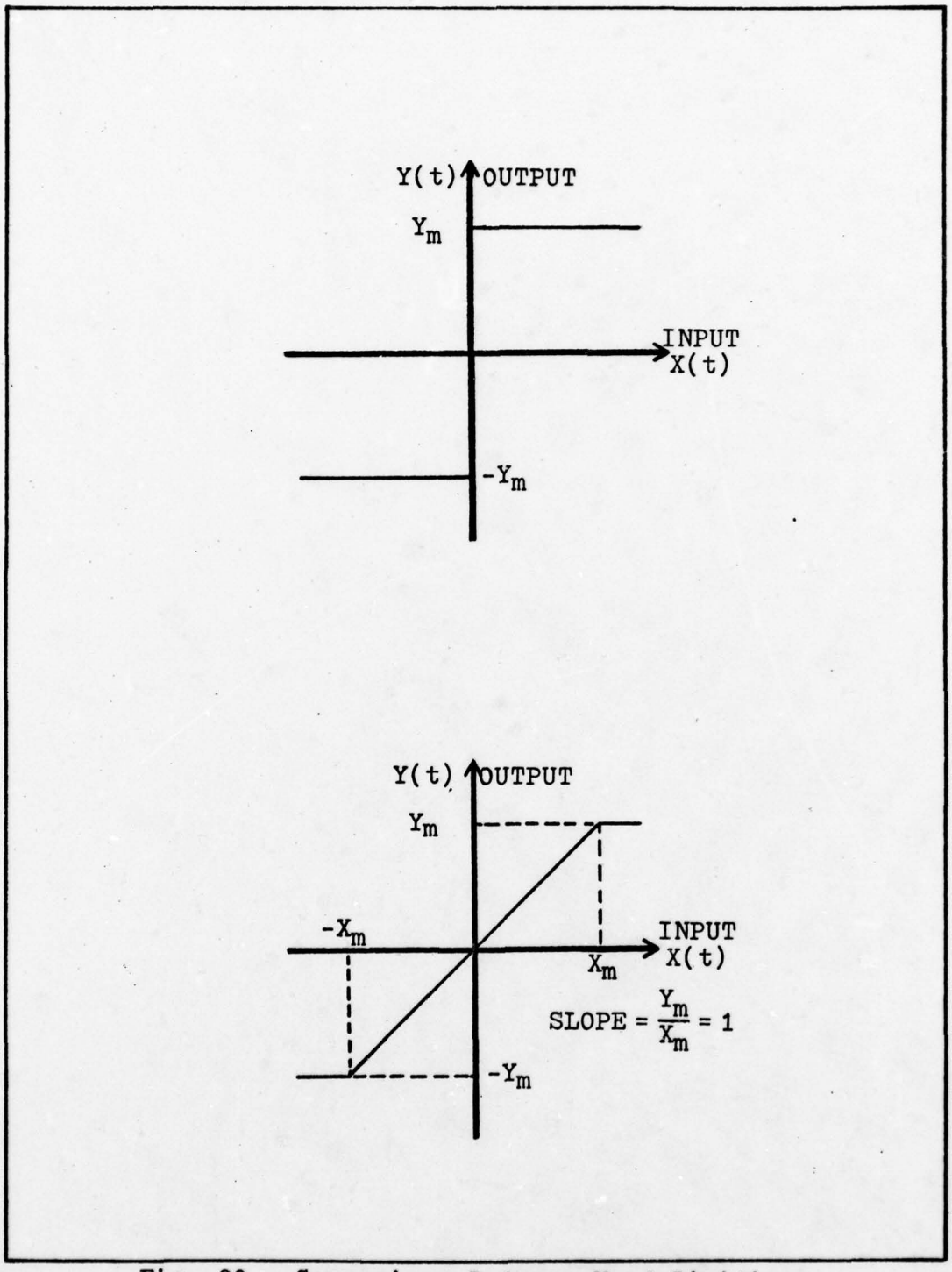


Fig. 20. Comparison Between Hard Limiting (Top) and Soft Limiting (Bottom).

is

$$s_{oc}(t) + js_{os}(t) = \frac{s_{ic}(t) + js_{is}(t)}{\sqrt{s^2_{ic}(t) + s^2_{is}(t)}} \tag{46}$$

where $s_c(t)$ is the I channel component, $s_s(t)$ the Q channel component, $\{j = \sqrt{-1}\}$, and "i" and "o" indicate input and output respectively.

The normalization process of a hard or soft limiter, or the action of any nonlinear device, generates nonlinear distortion. Nonlinear distortion can be described by a square-law transformation (Ref. 26:259) as

$$Z(t) = Y^2(t) \tag{47}$$

where Y(t) is the input waveform and Z(t) is the distorted output waveform. Applying equation (23), the common expression for OQPSK, MSK and SFSK, to equation (47) and using trigonometric identities, the output can be written as

$$Z(t) = \tfrac{1}{2}[C^2(t)+S^2(t)]+\tfrac{1}{2}[C^2(t)-S^2(t)]\text{Cos}(2W_c t) - [d_k C(t)S(t)]\text{Sin}(2W_c t) \tag{48}$$

Thus, nonlinear distortion produces frequencies at the output of a device other than frequencies of the input. Equation (48) consists of a low frequency input data dependent term and two modulated terms at the first harmonic of the input carrier frequency. Evaluating equation (48) for the symbol pulse sequences of OQPSK, MSK and SFSK gives

$$Z_{OQPSK}(t) = 1-d_k\text{Sin}(2W_c t) \tag{49}$$

$$Z_{MSK}(t) = \tfrac{1}{2}+\text{Cos}(\tfrac{\pi}{T}t)\text{Cos}(2W_c t)-d_k\text{Sin}(\tfrac{\pi}{T}t)\text{Sin}(2W_c t) \tag{50}$$

$$Z_{SFSK}(t) = \frac{1}{2}+\cos\left[\frac{\pi}{T}t-\frac{1}{2}\sin\left(\frac{2\pi}{T}t\right)\right]\cos(2W_c t)$$

$$- d_k \sin\left[\frac{\pi}{T}t-\frac{1}{2}\sin\left(\frac{2\pi}{T}t\right)\right]\sin(2W_c t) \qquad (51)$$

Equations (49), (50) and (51) reveal that all harmonic distortion terms for these three types of modulation are modulated by the input data sequence d_k, or a shaped data sequence at the input data rate. This last observation is of particular interest for application of OQPSK, MSK and SFSK to spread-spectrum.

Application of Filtering and Limiting OQPSK, MSK and SFSK

In this section a three step procedure is used to analyze the practical application of filtering and limiting the envelopes of OQPSK, MSK and SFSK. First, the amplitude and phase characteristics of each modulation type are developed. Next, the envelopes of each are applied to a filter, then to a filter and limiter combination. The combined filter and limiter configuration is as shown in Figure 21. Finally, where available, simulated or measured power spectral densities of the various combinations are given.

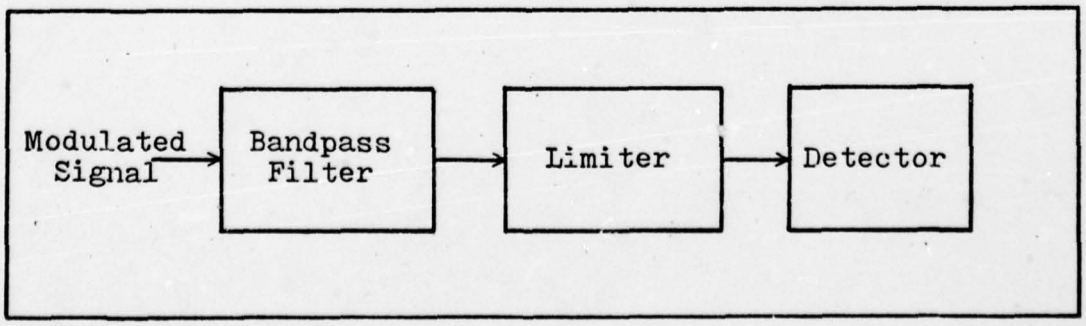


Fig. 21. Combined Filter and Limiter Configuration

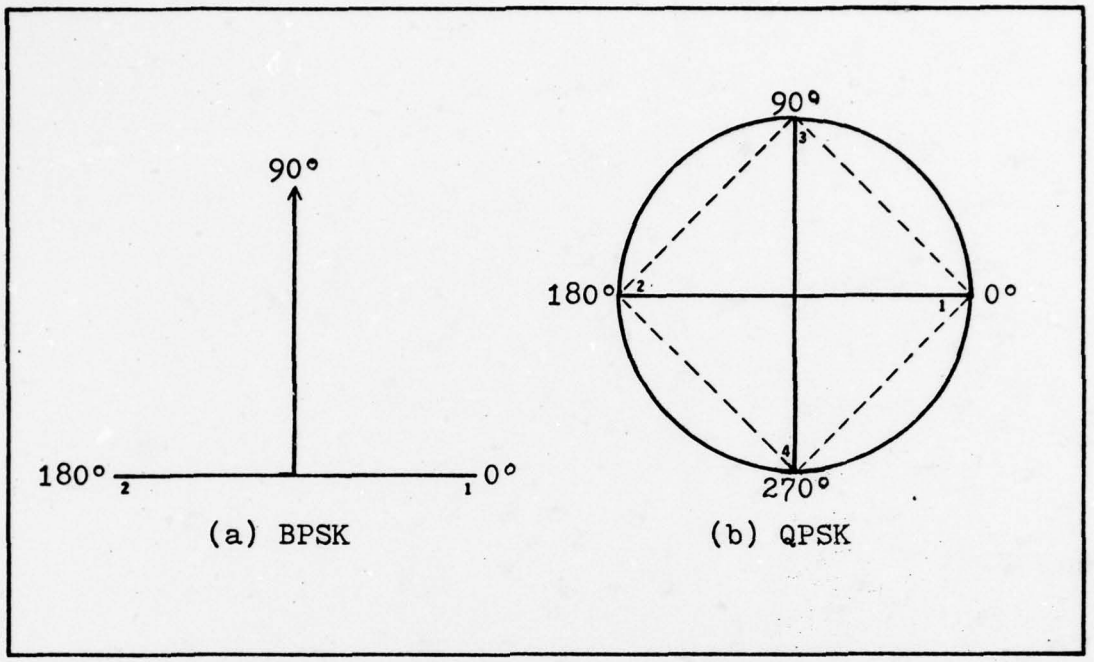


Fig. 22. Phasor Diagrams of BPSK and QPSK Phase Transitions

OQPSK Amplitude and Phase Characteristics. The amplitude and phase characteristics of OQPSK can best be developed by first looking at the amplitude and phase characteristics of BPSK and QPSK. Binary Phase Shift Keying has only two phase states, 0° and 180°, as shown in Figure 22(a). In order to change from state 1(2) to state 2(1), the phase vector traverses the line from point 1(2) to 2(1) passing through zero amplitude along the way. The phase transitions are instantaneous and occur as the amplitude of the envelope passes through zero.

Quadriphase Shift Keying, as discussed in Chapter 2 can be viewed as consisting of two overlapping BPSK channels (channels I and Q) of the same frequency in phase quadrature.

The phase transitions of the two channels occur simultaneously, resulting in phase shifts of 0°, ± 90°, and 180° for the QPSK envelope. Figure 22(b) shows a phasor diagram of the phase states of QPSK. A phase transition from state 1 to state 3 can be accomplished by reducing the 0° vector to zero amplitude and increasing the 90° vector to full amplitude. If these two operations are performed simultaneously, the phase vector will traverse the path shown as a dotted line from state 1 to state 3. This phase vector does not pass through zero amplitude and indeed only suffers a 3dB drop in amplitude during the transition. During a 180° phase transition, however, the phase vector does pass through zero amplitude just as in BPSK. Thus, the 90° phase transition occurs at a much slower rate than the instantaneous 180° phase transition. Offset QPSK (OQPSK) has the restriction that phase transitions can only occur in 90° increments, thus avoiding the zero amplitude problem of PSK and QPSK.

Filtered OQPSK. The effects of filtering a OQPSK envelope will be developed by first looking at the effects of filtering QPSK. Filtering a QPSK envelope with a filter whose bandwidth is on the order of the signalling rate (BT product = 1) results in the output symbol pulses (symbol pulses of the modulated carrier wave) experiencing intersymbol interference. The nature and magnitude of the interference is dependent upon the rate-of-change in amplitude and phase at the transition intervals, and in

the similarity between the pulses preceding and following the transition intervals. This can be illustrated by analyzing the 180° and 90° phase transitions.

For a 180° phase transition of a QPSK envelope, both BPSK channels must change states, thus, the two adjacent output symbol pulses surrounding the transition can be thought of as having identical phases, but opposite polarities for the magnitudes. Hence, the smearing of two such pulses into each other because of nonlinear filtering results in destructive interference. At any point at which output symbols of opposite polarity overlap, the amplitude of the signal will be given by the difference in magnitude of the two pulses. Additionally, due to the rounding of the edges of the output symbol pulses from filtering, the amplitude of the envelope is reduced in the overlap region. About midway between the center of the symbol pulses, the magnitude of the two pulses are equal and cancel because of their opposite polarities. Thus, the envelope goes to zero at this point.

Since the phase vector from the two output symbol pulses of opposite polarity is equal to that of the larger component, the 180° phase transition is still instantaneous, and occurs at the point where the magnitude of the two pulses are equal and cancel. This rapid phase change produces high frequencies that are outside of the desired transmission range. However, because of the envelope droop resulting from the rounding of the output symbol pulses, there is very little power associated with the high frequency content, as

would be expected for a filtered signal.

For a 90° phase transition, only one BPSK channel must change state, thus, the instantaneous polarity change of the 180° phase transition is avoided. For this phase transition, the intersymbol interference created by nonlinear filtering is not destructive but vectorally additive. That is, the envelope of the signal at a region of two overlapping output symbol pulses with relative phase of 90° is equal to the RMS value of the magnitude of each pulse (Ref. 19). Let the magnitude of two such overlapping pulses be denoted by $V_n(t)$ and $V_{n+1}(t)$. Then the envelope of the sum is given by

$$V(t) = \sqrt{V^2_n(t) + V^2_{n+1}(t)} \tag{52}$$

Due to the rounding of the output symbol pulses as a result of filtering, the envelope will droop slightly in the region of a 90° phase transition.

Since the two BPSK channels are in phase quadrature, the phase vector at any time "t" can be determined from

$$\theta(t) = \tan^{-1} \frac{V_{n+1}(t)}{V_n(t)} \tag{53}$$

which is analogous to equation (2) given in Chapter 2 for input symbol pulses. With the output symbol pulses V_n and V_{n+1} smeared into each other by nonlinear filtering, the inverse tangent function will shift fairly smoothly from about 0° at the center of the nth output symbol pulse to 90° at the center of the (n+1)th output symbol pulse. Hence, the phase transition will be accomplished gradually for a filtered signal that undergoes a phase shift of 90°.

Since the slope $\frac{d\theta}{dt}$ of the phase will be small at all points within the transition region, the 90° phase change will not produce high frequencies.

Filtered and Limited OQPSK. The effects of hard limiting a filtered OQPSK envelope (circuit configuration is illustrated in Figure 21) will be developed by contrast with a filtered and limited QPSK envelope. Hard limiting restores the envelope for both QPSK and OQPSK, but for QPSK the result is quite different.

For QPSK, when the envelope is restored by hard limiting, the instantaneous phase transitions and zero amplitude values from the 180° phase shifts result in large amounts of out-of-band interference. In fact, the restoration to a flat envelope by hard limiting yields rectangular output symbol pulses which are identical to the symbol pulses prior to filtering. Consequently, it is seen that hard limiting completely removes any bandlimiting effected by filtering the 180° phase transition for QPSK envelopes (Ref. 1:319).

For OQPSK, when the envelope is restored by hard limiting, the slow phase transitions result in virtually no increase in out-of-band interference. The limiting affects primarily only the envelope, leaving the phase relatively preserved. Consequently, out-of-band interference can be suppressed if 180° phase transitions are avoided.

The predicted effects of filtering and limiting QPSK

and OQPSK envelopes are verified by Figures 23 and 24[9]. As can be seen, the unfiltered power spectrums for QPSK and OQPSK are identical as stated in Chapter 3. Likewise the power spectra of the two envelopes are identical after bandlimiting with a filter on the order of the signalling rate (BT = 1). Note, however, in Figure 24 that after hard limiting the spectrum for OQPSK signalling remains at approximately its filtered value for frequencies greater than 2R, while the spectrum for QPSK is almost completely restored. For frequencies less than 2R, an undesired change not predicted has occured to the power spectrum of OQPSK. The main lobe initially reduced in width by filtering is restored approximately to its original value by hard limiting. This characteristic will have a limiting effect on the ability to filter an OQPSK waveform with BT<<1. Figure 25 is a plot for BT = 0.5.

The tremendous difference in intersymbol interference noted between QPSK and OQPSK has also been observed for PSK and an offset version of PSK known as Quadrature Clock Modulation (QCM) (Ref. 27). Quadrature Clock Modulation is a BPSK modulation technique in which 180° phase transitions have been eliminated. The technique used to eliminate 180° phase transitions and generate QCM is almost identical to

---

[9]Figures 23, 24 and 25 were extracted from reference 19. The figures were produced through computer simulation using a 4-pole Butterworth filter and a hard limiter. An input data rate of R = 64 was used, however, due to the method of display, the input data rate can be treated as R = 124 with f = 512 corresponding to 4R.

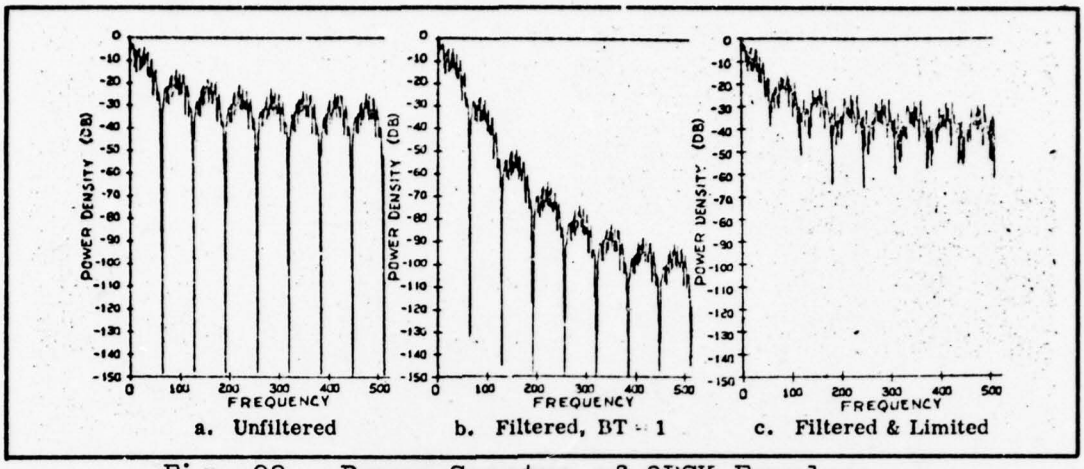


Fig. 23. Power Spectra of QPSK Envelope.

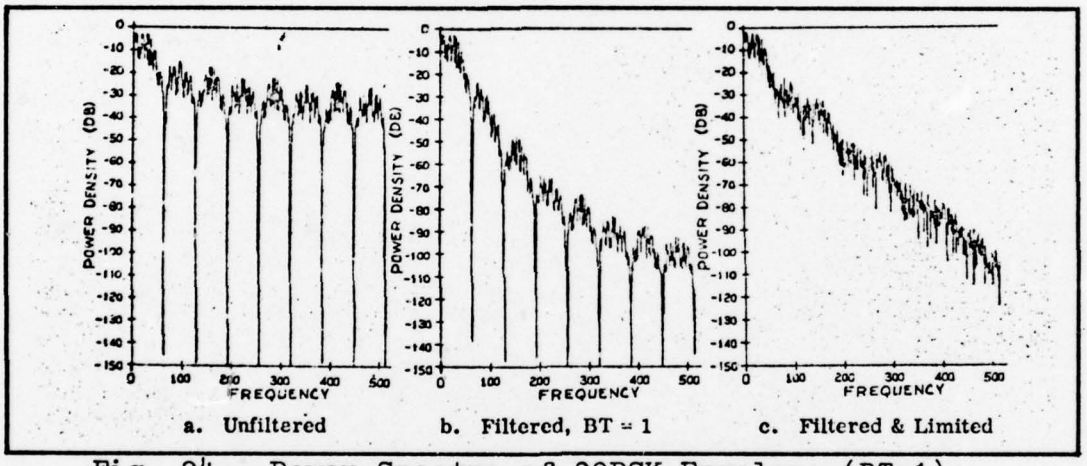


Fig. 24. Power Spectra of OQPSK Envelope (BT=1).

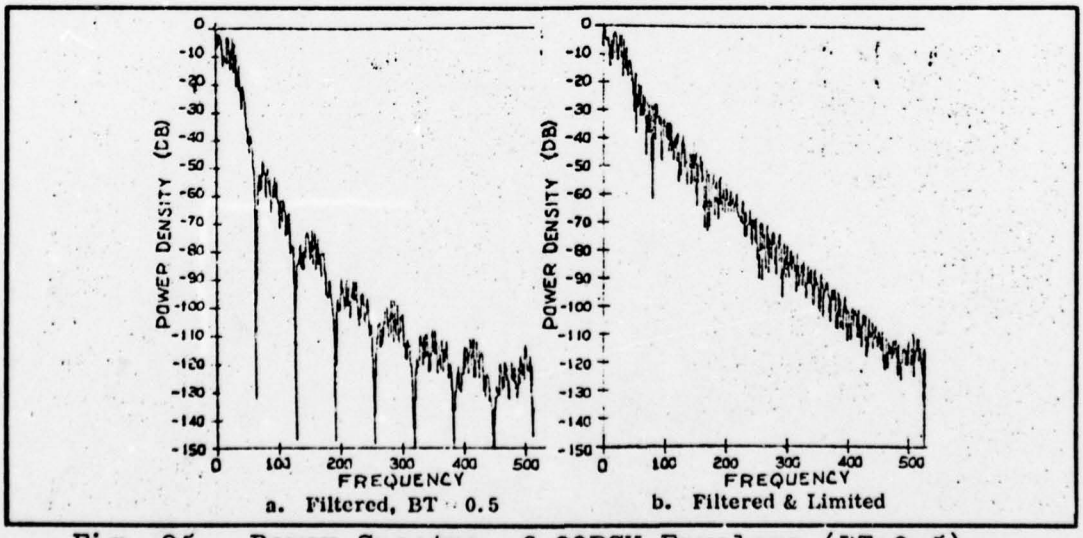


Fig. 25. Power Spectra of OQPSK Envelope (BT=0.5).

the method used for OQPSK, and results in phase transitions of ± 90°. In comparing QCM and BPSK, the article noted that for BT products of 1.5 or less, that QCM generated less intersymbol interference than BPSK, and consequently had a lower probability of bit error. For a probability of bit error of 10^{-5}, BPSK required 1.5dB, 3dB and 25dB increases in $\frac{E_b}{N_o}$ (ratio of required energy per bit to noise power density) over that of QCM, for BT products of 1.5, 1.0 and 0.5 respectively.

MSK Amplitude and Phase Characteristics. The power spectrum of MSK rolls off more rapidly than the spectrum for OQPSK. The suppression of high frequencies is a result of the continuous phase transitions at the bit transition intervals and the piecewise linear phase function during the intervals. At the bit transition intervals, the frequency change is instantaneous, however, the resulting envelope has a constant magnitude since $C^2(t) + S^2(t) = 1$. The input symbol pulses C(t) and S(t) for MSK are given by equation (18) in Chapter 2.

Filtered MSK. Filtering a MSK envelope with a filter whose bandwidth is on the order of the signalling rate results in rounding of the V-shaped corners of the phase when the phase slope reverses polarity (see Figure 5 in Chapter 2). Hence, the phase transitions will be accomplished gradually for a filtered signal, and since the slope $\frac{d\theta}{dt}$ of the phase will be small at all points within the transmitted region, high frequencies will not be

produced. The filtering process has very little effect on the amplitude of the waveform and causes only slight droops in its magnitude at the regions of the V-shaped phase corners. Consequently, the effects of filtering a MSK envelope is essentially restricted to the smoothing of phase transitions (Ref. 19).

Filtered and Limited MSK. Hard limiting a filtered MSK waveform (circuit configuration is illustrated in Figure 21) results in the restoration of the envelope. The restoration in this case consists basically in the removal of the slight amplitude droops. Hence, the smooth phase transitions introduced by filtering remain, and out-of-band interference is not produced.

The predicted effects of filtering and limiting a MSK waveform are verified by Figure 26[10] and 27[11]. As can be seen, the power spectrum after filtering and limiting is approximately the same as the spectrum after filtering alone. However, an undesired change not predicted has occured to the power spectrum. The main lobe initially reduced in width by filtering is restored approximately to its original value

---

[10]Figure 26 was extracted from reference 19. This figure was produced through computer simulation using a 4-pole Butterworth filter and a hard limiter. An input data rate R = 64 was used, however, due to the method of display the input data rate can be treated as R = 124 with f = 512 corresponding to 4R.

[11]Figure 27 was extracted from reference 9. This figure was produced through simulation of a satellite link by using a transmit bandlimiting filter and a hard limiter interposed between an ideal modulator and demodulator. The notation R_L is the input data rate, while B_T is the 3dB bandwidth of the filter.

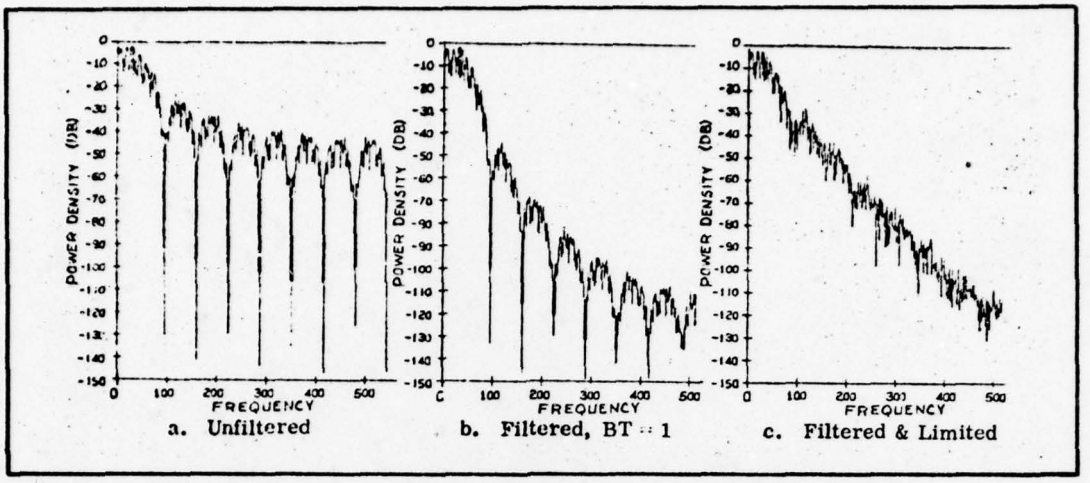


Fig. 26. Power Spectra of MSK Envelope

by hardlimiting. This characteristic will make it difficult to use MSK in applications requiring a bandwidth less than or equal to the data rate, since the single sided bandwidth for the main lobe is equal to 0.75R.

SFSK Amplitude and Phase Characteristics. The power spectrum of SFSK rolls off more rapidly than the spectrums of OQPSK or MSK. The suppression of high frequencies is a result of the properties of both frequency and phase. Frequency and phase both possess linear transitions (continuous frequency and phase) at bit transition intervals, zero rates-of-change approaching and leaving bit transition intervals, and continuous rates-of-change within bit intervals. Since neither frequency nor phase have abrupt changes, the generation of high frequencies is only minimal. The waveforms for frequency and phase are plotted in Figures 7 and 8 of Chapter 2. Sinusoidal Frequency Shift Keying has a constant envelope since $C^2(t) + S^2(t) = 1$. The input symbol pulses C(t) and S(t) for SFSK are given by equation (22) in Chapter 2.

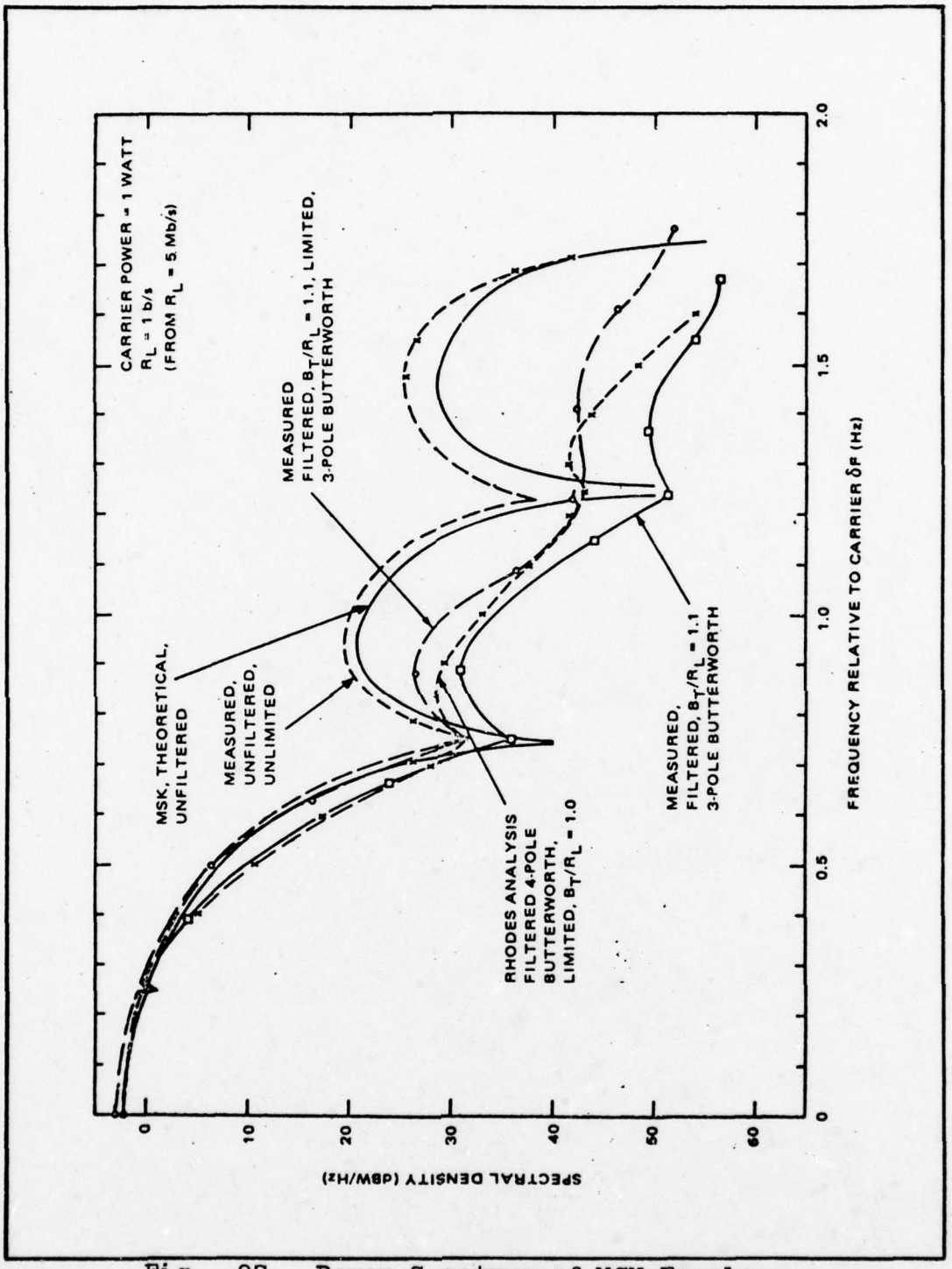


Fig. 27. Power Spectrum of MSK Envelope.

Filtered SFSK. Filtering a SFSK waveform with a filter whose bandwidth is on the order of the signalling rate results in further smoothing of the phase waveform. The filtering process tends to reduce the maximum rate-of-change in phase during the bit intervals, and to smooth the ripple in the phase waveform at the transition intervals, when the polarity of the phase has not changed. In many respects, the resulting phase waveform of a filtered SFSK signal resembles the phase waveform of a filtered MSK signal. Hence, the phase shape of a filtered SFSK waveform will be smoother than the unfiltered phase waveform, and since the maximum slope $\frac{d\theta}{dt}$ has been reduced, less high frequencies than before will be generated. The filtering process has very little effect on the amplitude of the waveform, thus creating only slight droops in the amplitude corresponding to where the phase waveform was smoothed.

Filtered and Limited SFSK. Hard limiting a filtered SFSK waveform (circuit configuration is illustrated in Figure 21) results in removal of the envelope amplitude droops. Hence, the smooth phase waveshape introduced by filtering remains, and only a very slight increase in the level of out-of-band frequency is generated. The power spectrums of and limited SFSK waveforms are projected to be similar to, but of greater roll off than, those of MSK. Additionally, the effects of filtering and limiting the main lobe of SFSK are expected to be greater than those of OQPSK and MSK, since the single sided bandwidth of SFSK is 0.86R.

Published results of filtering and limiting SFSK waveforms are not currently available. However, the principles used above in the theoretical development have been verified many times.

Probability of Error

Performance comparisons will be made in this section by using probability of error as the basic figure of merit. An ideal channel will be considered first, then a realistic bandlimited nonlinear channel will be considered.

Ideal Channel. The probability of error of QPSK, OQPSK, MSK and SFSK on an ideal channel is of interest for relative comparison. An ideal channel is defined as a linear, infinite bandwidth channel, corrupted only by additive white gaussian noise (WGN) (Refs. 4 and 5). In addition, perfect carrier and timing references are assumed available at the receiver. With these assumptions, and viewing QPSK, OQPSK, MSK and SFSK as orthogonal binary channels with antipodal signalling, the binary error probability (Ref. 28) is

$$P_e = \int_{\lambda}^{\infty} \frac{1}{\sqrt{2\pi}} e^{-y^2/2} \, dy \qquad (54)$$

where

$\lambda = \sqrt{2E_b/N_o}$

E_b/N_o = ratio of required energy per bit to noise power density

Therefore, on an ideal channel, given the same transmission power for QPSK, OQPSK, MSK and SFSK, and the same data input

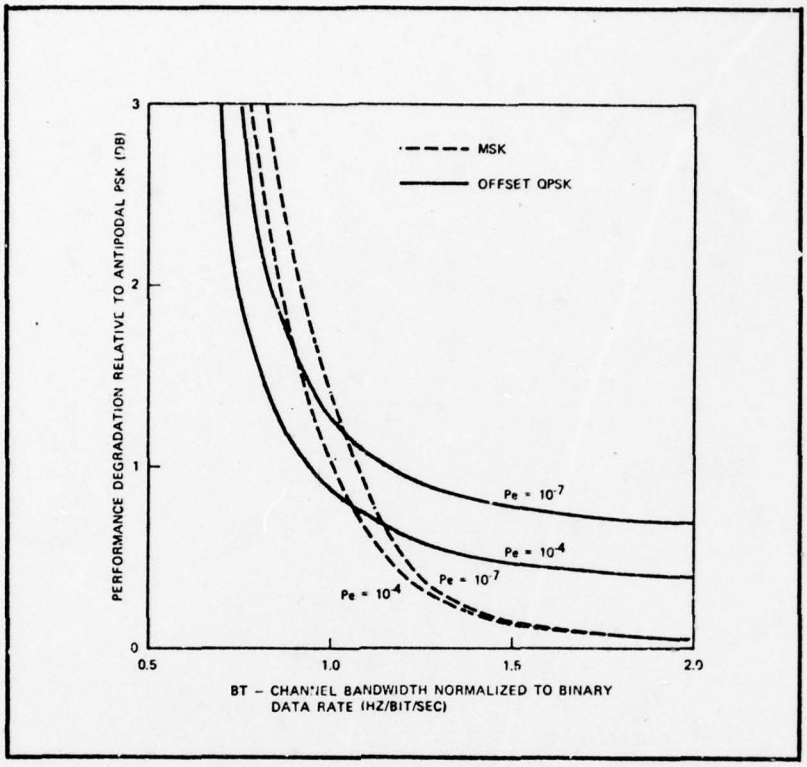


Fig. 28. MSK and OQPSK E_b/N_o Performance Degradation With Respect to Ideal Antipodal PSK.

rate R, the probability of errors for each modulation type are equal. This is because for a given R, the signalling rates of each modulation type as shown in Chapter 2 are equal. However, on a realistic channel, the probability of error for each modulation type is effected by filtering, limiting and nonlinear circuit elements.

Realistic Channel. This section will consider measured performance of QPSK, OQPSK and MSK on bandlimited nonlinear channels. Performance results of SFSK on bandlimited nonlinear channels are not currently available.

Figure 28 is from Gronemeyer and McBride (Ref. 5) and shows E_b/N_o performance degradation verses BT with

respect to antipodal PSK for OQPSK and MSK. These results were obtained by computer simulation of a bandlimited nonlinear satellite communication system. The simulated system consisted of two 7-pole, 0.1dB ripple Chebyshev complex envelope filters, a bandpass hard limiter (see equation (46)), and two WGN sources. Performance degradation is defined as the ratio of the total link E_b/N_o required on the simulated link to achieve the desired bit error rate (BER) to the E_b/N_o required on an infinite bandwidth, WGN channel to achieve the same BER (Ref. 5). The channel bandwidth B is defined as the noise bandwidth of the two identical filters in cascade.

Gronemeyer and McBride's assessment of the results presented in Figure 28 are as follows: "The performance curves show a crossover point, such that for channel bandwidths exceeding approximately 1.1R, where R is the binary data rate, the performance of MSK is superior to that of Offset QPSK. Conversely, for B<1.1R, Offset QPSK has an advantage over MSK. The reason for the performance crossover is basically the narrower main lobe of the spectral density of Offset QPSK as compared to MSK. Both techniques begin to suffer severe degradation as their main spectral lobes encounter the channel band edge. Since the main lobe of MSK is wider than that of Offset QPSK, MSK begins to degrade sooner than Offset QPSK as channel bandwidth is decreased."

Figures 29, 30, and 31, from Taylor, Chan and Haykin

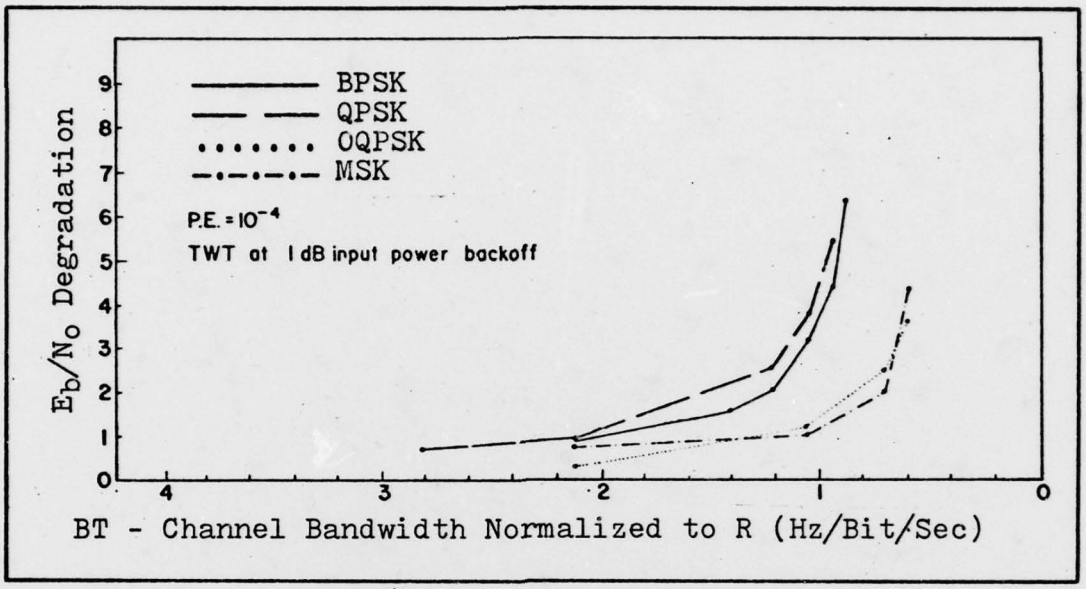


Fig. 29. E_b/N_o Performance Degradation.

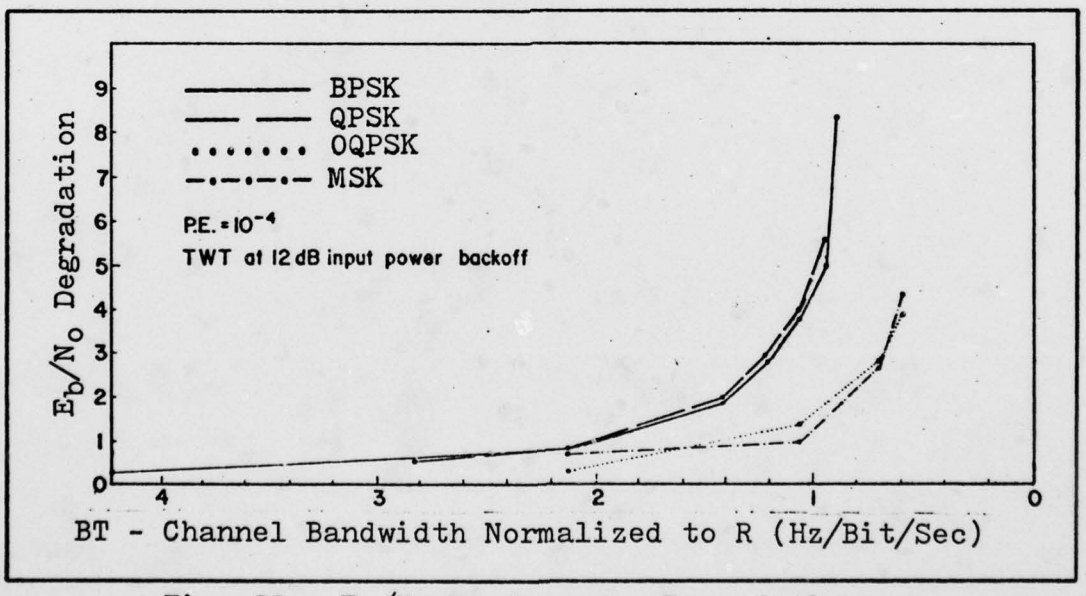


Fig. 30. E_b/N_o Performance Degradation.

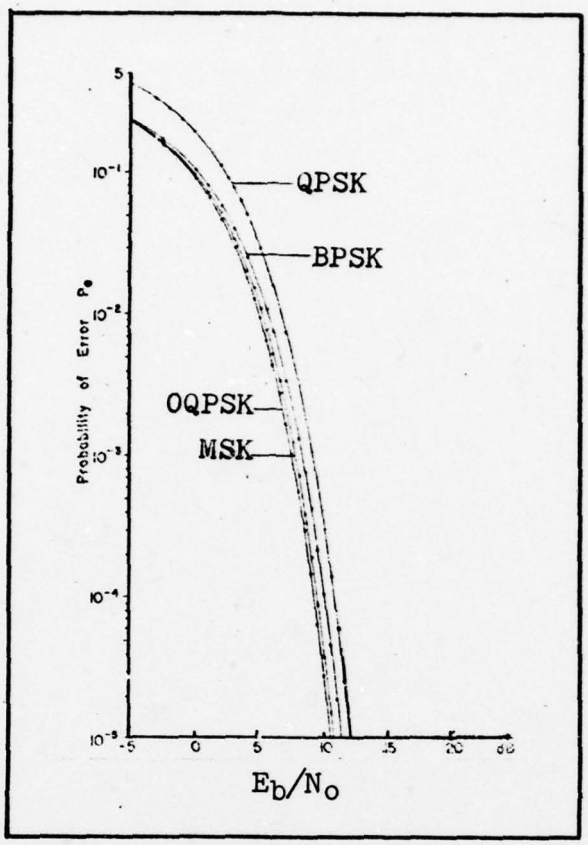


Fig. 31. Probability of Error for BT = 1.3R and 1dB Input Backoff.

(Ref. 6), compare probability of error between PSK, QPSK, OQPSK and MSK. Figures 29 and 30 show E_b/N_o performance degradation verses BT for a probability of error equal to 10^{-4}, while Figure 31 shows probability of error verses E_b/N_o for BT = 1.3R. These figures were obtained by computer simulation of a bandlimited nonlinear satellite communication channel. The simulated channel consisted of a cascade combination of two 4-pole, 0.5dB ripple Chebyshev complex envelope filters and a nonlinear traveling wave tube (TWT). The channel bandwidth B is defined by the authors as the 3dB noise bandwidth of the two identical filters in cascade.

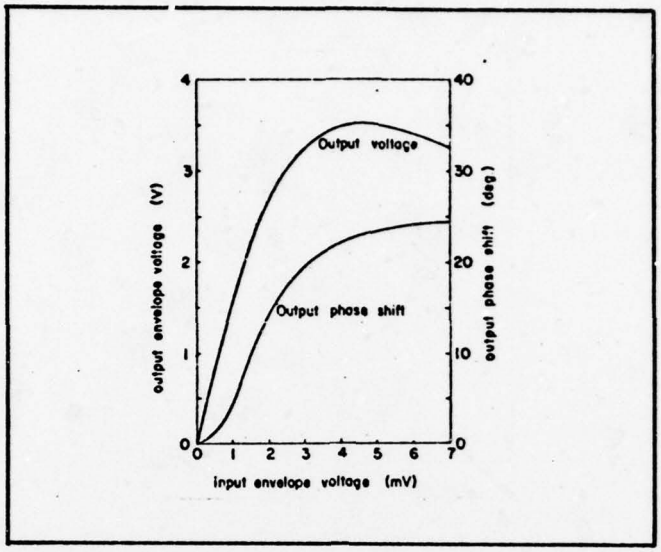


Fig. 32. Voltage and Phase Transfer Characteristic for a Hughes 261-H TWT.

The TWT sinulated was the Hughes 261-H tube with voltage and phase characteristics as shown in Figure 32. The Hughes TWT is nonlinear, and exhibits both a gain compression or soft limiting effect and an amplitude to phase conversion (AM/PM) effect. Both of these effects may cause significant nonlinear signal distortion with a corresponding degradation in communication system performance. The operating conditions of a TWT are described by the ratio of its actual input power Pin to the maximum input power Pmax. This ratio when expressed in dB is referred to as the input power backoff P_b (Ref. 25) of the TWT, and expressed mathematically as

$$P_b = -10 \log_{10} \frac{Pin}{Pmax} \qquad (55)$$

Two operating points of the tube were used in the simulation; one at an input power backoff of 12dB, and the second at 1dB.

At 12dB input power backoff, the TWT is operating in the linear region, and at 1dB input power backoff it is essentially in saturation.

From Figures 29, 30 and 31 it can be seen that OQPSK and MSK offer significantly less degradation from ideal than PSK or QPSK when filtered and limited with a BT product less than 2R. Additionally, these curves show two performance crossover points for OQPSK and MSK, with OQPSK providing the best probability of error performance for BT products greater than about 1.3R and less than about 0.65R. Only minor differences were noted in E_b/N_o degradation or bit error performance for the two values of TWT input power backoff.

Figures 33 and 34, from Fielding, Berger and Lochhead (Ref. 29), compare bit error rate probability verses E_b/N_o for OQPSK and MSK. These results were obtained by the use of a 650 MHz wide Ku-band demonstration link. Bit error rate measurements were made for modulator-demodulator, and end-to-end link configurations with data rates of 600 and 800 Mbps. For an input of 600 Mbps, the BT product equals 1.08R, while for R = 800 Mbps, the BT product equals 0.81R.

The measured E_b/N_o for a bit error rate of 10^{-5} is summarized in Table II and the differential degradation (end-to-end relative to modulator-demodulator) is summarized in Table III. For this particular system the differential degradation with MSK is only slightly less than OQPSK. However, for the modulator-demodulator alone, the absolute degradation for MSK is 1.6 and 1.2dB less than OQPSK at 600 and 800 Mbps, respectively.

TABLE II

Summary of Required E_b/N_o for

a Bit Error Rate of 10^{-5}

DATA RATE (Mbps)	OQPSK (dB)		MSK (dB)	
	Mod-Demon	End-to-End	Mod-Demon	End-to-End
600	12.25	13.35	10.65	11.55
800	12.60	15.10	11.45	13.75

TABLE III

Summary of Differential Degradation

for a Bit Error Rate of 10^{-5}

DATA RATE (Mbps)	OQPSK (dB)	MSK (dB)
600	1.1	0.9
800	2.5	2.3

In this chapter the performance of OQPSK, MSK and SFSK was evaluated using practical channel conditions. This evaluation was performed first by considering the linear and nonlinear characteristics of the system devices on an individual basis and as applied to each modulation type, then by comparing simulated or measured probability of errors for various modulation types.

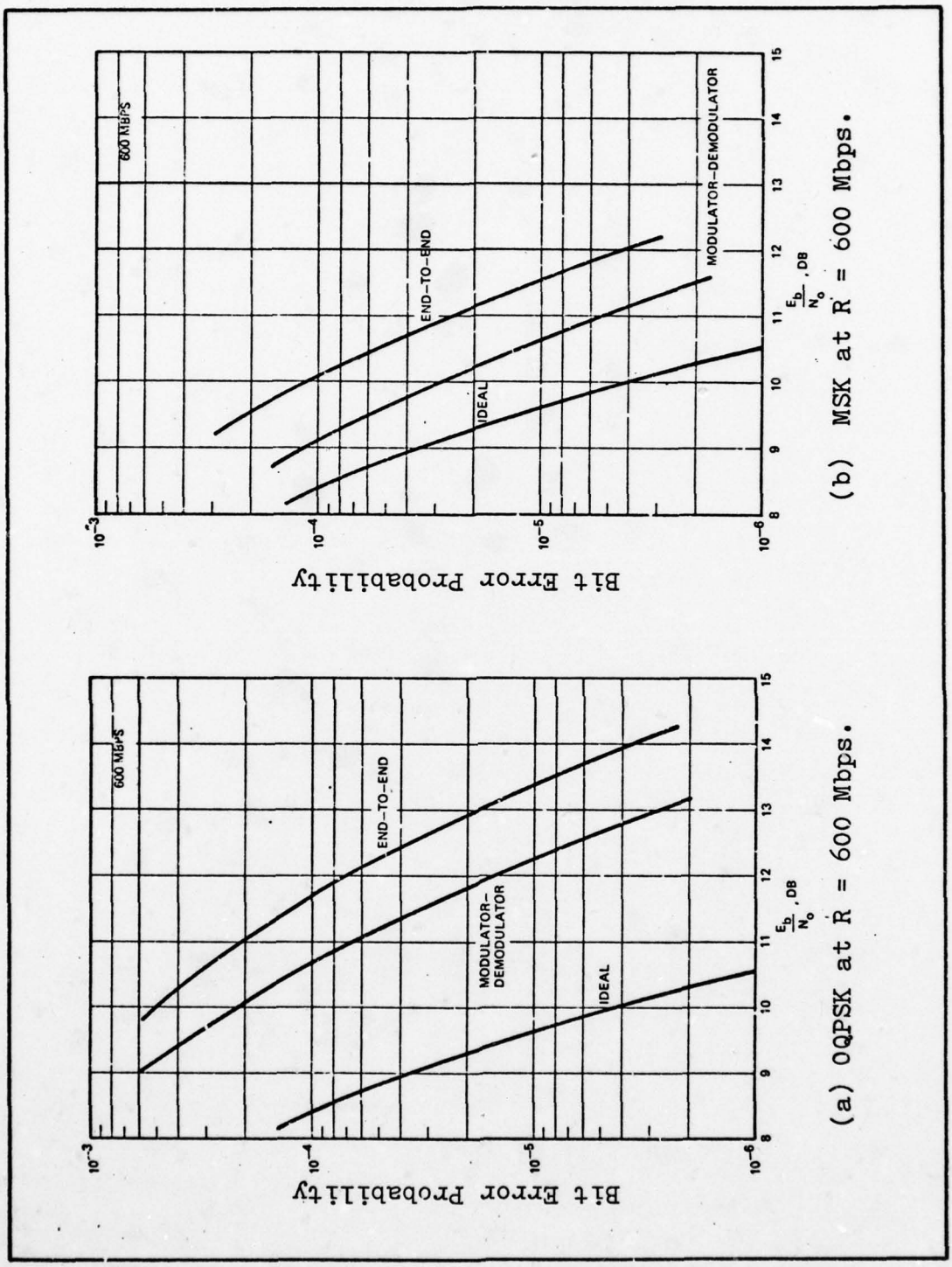


Fig. 33. Bit Error Performance for BT = 1.08R.

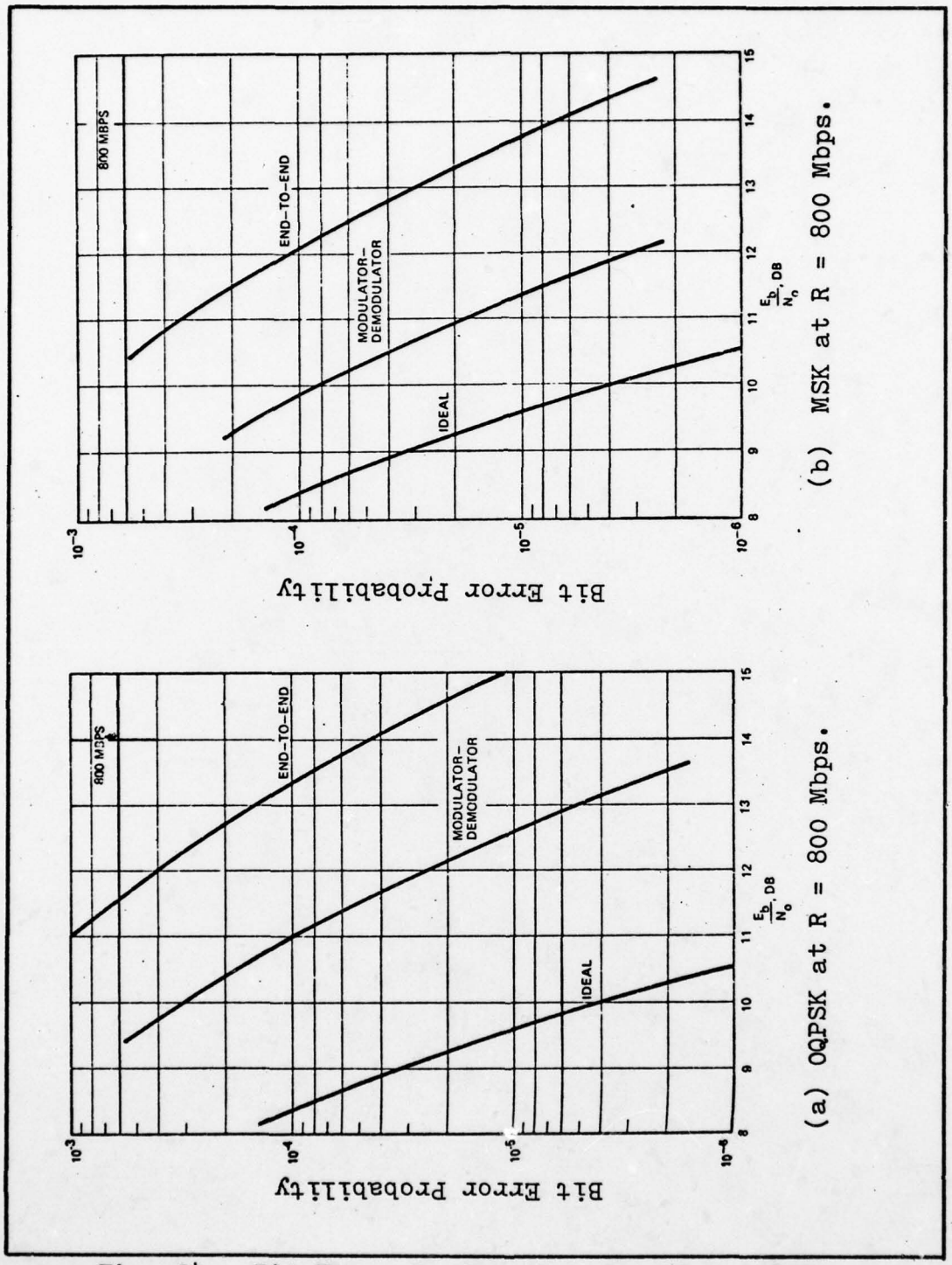


Fig. 34. Bit Error Performance for BT = 0.81R.

V Conclusions and Recommendations

Conclusions

Offset QPSK, MSK and SFSK have been evaluated both graphically and mathematically, and compared to more fundamental modulation techniques. A common mathematical relationship was developed between the three modulation types, and it was shown that the three types are mathematically identical, except for the shape of the input symbol pulses, when viewed as inphase and quadrature phase channels employing offset, time-shifted symbol pulses. The input symbol pulses for OQPS, MSK and SFSK are rectangular, sinusoidal and raised-cosine in shape, respectively.

A first-order Markov process model was used to compute the autocorrelation functions, while the power spectral densities were computed by taking the Fourier transforms of the autocorrelation functions. The roll off characteristics of the power spectral densities for OQPSK, MSK and SFSK were determined to be $(f/R)^{-2}$, $(f/R)^{-4}$ and $(f/R)^{-8}$ respectively for large values of f/R, with the first nulls falling at f/R = 0.50, 0.75 and 0.86 respectively. The theoretical spectral occupancy of each modulation technique was computed by two methods; the out-of-band power ratio, and the mean-square crosstalk between two channels of like modulation. Both measurement methods revealed similar, but not identical crossover points in the performance curves of

the three modulation techniques.

The out-of-band performance curves indicated that for a BT product exceeding about 3.0R, SFSK has lower fractional out-of-band power than MSK or OQPSK, while for a BT product between 3.0 to 1.5R MSK has the lowest fractional out-of-band power. However, as the BT product is decreased below 1.0R, a point is reached ($\approx$0.7R) where OQPSK has fractional out-of-band power lower than MSK or SFSK.

The mean-square crosstalk performance curves indicated that for channel separations greater than about 2.3R, two SFSK channels have less mean-square crosstalk than two channels of MSK or OQPSK, while for channel separations between about 0.75 and 2.3R two MSK channels have the lowest mean-square crosstalk. However, for channel separations less than 0.75R, two OQPSK channels have the lowest mean-square crosstalk.

The relationship between the shape of the power spectral density to the shapes of the autocorrelation function and the input symbol pulse was analyzed and evaluated. It was shown that the width of the main lobe of the power spectrum and the spectral roll off are both directly related to the tangency (smoothness) of the symbol pulse and the autocorrelation function.

An analysis of the bit error rates of OQPSK, MSK and SFSK lead to consideration of both theoretical and practical channel conditions. The bit error rates of OQPSK, MSK and SFSK on an ideal channel are theoretically equal

and determined solely by the received ratio E_b/N_o. Additionally, these bit error rates are identical to the bit error rates of PSK and QPSK. However, in a nonlinear band-limited channel, these relationships do not hold true, and the bit error performance is a function of the channel bandwidth and the degree of nonlinearity within the channel.

In analyzing the simulated and measured bit error performance curves of OQPSK and MSK, the following observations were made: (1) For BT products less than 2R, OQPSK and MSK offer significantly less degradation than PSK or QPSK. (2) Offset QPSK and MSK are both relatively immune to system nonlinearities. (3) For BT products between 2R and 0.6R, OQPSK and MSK offer about the same bit error performance. Various bit error performance crossover points exist between the two within this range depending upon the system configuration and the degree of nonlinearity, however, the bit error rates are within 1dB of each other. (4) For BT products less than 0.6R, both OQPSK and MSK begin to suffer severe degradation, with the degradation of MSK being the greatest.

Simulated and measured bit error performance curves for SFSK are not currently available for evaluation and comparison. However, in consideration of the known characteristics of SFSK and its many similarities to OQPSK and MSK, the bit error rate of SFSK is expected to be compariable to the bit error rates of OQPSK and MSK.

Recommendations

It is the recommendation of the author that four other aspects of OQPSK, MSK and SFSK be analyzed. First, investigate through simulation or experimentation the probability of error and spectrum shaping resulting from filtering and limiting a SFSK modulated waveform. These results were not available in literature for inclusion in this report, and are necessary to complete the comparison. Second, an evaluation of the bit error performance of OQPSK, MSK and SFSK for noisy phase reference sources and synchronization errors. In the analysis and comparisons made within this report, all levels of synchronization were assumed available at the receiver; however, synchronization problems and noisy phase references exist to some degree in all practical communications systems. Next, the cost and complexity of transmitter and receiver structures should be investigated. These factors are often important considerations in determining a modulation type for an application. Finally, the performance of differentially encoded OQPSK (DOQPSK) (Ref. 1:313), phase comparison MSK (PCMSK) (Refs. 30 and 31) and phase comparison SFSK (PCSFSK) (Ref. 32) should be investigated. In the analysis and comparisons made within this report, an absolute phase reference source was assumed available at the receiver; however, in some applications, this is not true. Differentially encoded OQPSK is specifically designed for transmission of OQPSK to a nonsynchronous receiver, while PCMSK, and PCSFSK are nonsynchronous detection methods for MSK and SFSK respectively.

Bibliography

1. Spilker, James J. Jr. Digital Communications by Satellite. New Jersey: Prentice-Hall, Inc., 1977.

2. Anderson, Carl. "PSK Sidebands Reduced by Premodulation Filtering," Microwave Journal: 69-73 (January 1978).

3. Kalet, Irvin. "A Look at Crosstalk in Quadrature-Carrier Modulation Systems," IEEE Transactions on Communication, COM-25 9: 884-892 (September 1977).

4. Gronemeyer, Steven A. and Alan L. McBride. "Theory and Comparison of MSK and Offset QPSK Modulation Techniques Through a Satellite Channel," Proceedings of National Telecommunications Conference. 30/28-32. New Orleans, Louisiana: IEEE, December 1975.

5. -----. "MSK and Offset QPSK Modulation," IEEE Transactions on Communications, COM-24 8: 809-819 (August 1976).

6. Taylor, O.P., H.C. Chan, and S.S. Haykin. "A Simulation Study of Digital Modulation Methods for Wide-Band Satellite Communications," IEEE Transactions on Communications, COM-24 12: 1351-1354 (December 1976).

7. Ziemer, R.E. and W.H. Tranter. Principles of Communications. Boston: Houghton Mifflin Company, 1976.

8. Schonhoff, Thomas A. "Symbol Error Probabilities for M-ary CPFSK: Coherent and Noncoherent Detection," IEEE Transactions on Communications, COM-24 6: 644-652 (June 1976).

9. Mathwich, H. Robert, Joseph F. Balcowicz, and Martin Hecht. "The Effect of Tandem Band and Amplitude Limiting on the E_b/N_o Performance of Minimum (Frequency) Shift Keying (MSK)," IEEE Transactions on Communications, COM-22 10: 1525-1539 (October 1974).

10. Amoroso, Frank. "Pulse and Spectrum Manipulation in the Minimum (Frequency) Shift Keying (MSK) Format," IEEE Transactions on Communications, COM-24 3: 381-384 (March 1976).

11. Elsen, H.C. Van Den and P. Van Der Wurf. "A Simple Method of Calculating the Characteristics of FSK Signals with Modulation Index 0.5," IEEE Transactions on Communications, COM-20 2: 139-147 (April 1972).

12. Prabhu, Vasant K. "Spectral Occupancy of Digital Angle-Modulation Signals," Bell System Technical Journal, 55 4: 429-453 (April 1976).

13. Sullivan, W.A. "High-Capacity Microwave System for Digital Data Transmission," IEEE Transactions on Communications, COM-20: 466-470 (June 1972).

14. Trafton, Paul J. "Correlation Properties of MSK Sequences," Proceedings of National Telecommunication Conference. 554-559. San Diego, California: IEEE, December 1974.

15. Simon, Marvin K. "A Generalization of Minimum-Shift-Keying (MSK)-Type Signalling Based Upon Input Data Symbol Pulse Shaping," IEEE Transactions on Communications, COM-24 8: 845-856 (August 1976).

16. Reference Data for Radio Engineers. Howard W. Sams & Co., Inc. Sixth Edition, 1975.

17. Lindsey, William C. and Marvin K Simon. Telecommunication System Engineering. New Jersey: Prentice-Hall, Inc., 1973.

18. Stein, Seymour and J. Jay Jones. Modern Communication Principles. San Francisco: McGraw Hill, Inc., 1967.

19. Rhodes, S.A. "Effects of Hardlimiting on Bandlimited Transmissions with Conventional and Offset QPSK Modulation," Proceedings of National Telecommunication Conference. 20F/1-7. IEEE, 1972.

20. Mason, Samuel J. and Henry J. Zimmerman. Electronic Circuits, Signals, and Systems. New York: John Wiley & Sons, Inc., 1960.

21. Papoulis, Athanasious. Signal Analysis. San Francisco: McGraw Hill, Inc., 1977.

22. Kreyszig, Erwin. Advanced Engineering Mathematics: Third Edition. New York: John Wiley & Sons, Inc., 1972.

23. Prabhu, Vasant K. "PSK-Type Modulation with Overlapping Baseband Pulses," IEEE Transactions on Communications, COM-25 9: 980-990 (September 1977).

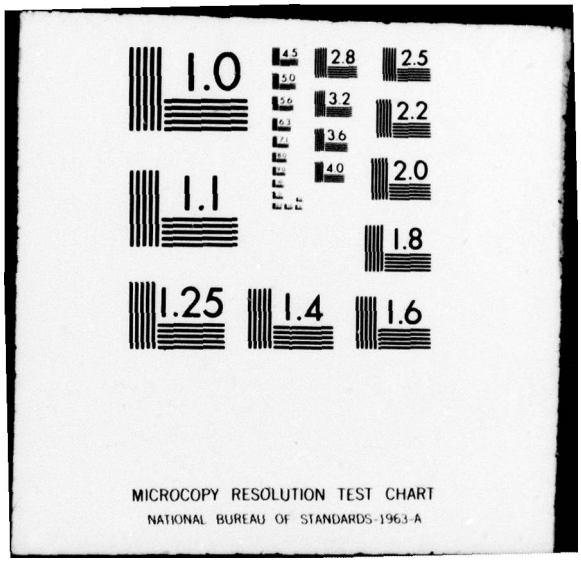
AD-A064 363 AIR FORCE INST OF TECH WRIGHT-PATTERSON AFB OHIO SCH--ETC F/G 9/3
ANALYSIS OF MODERN DIGITAL MODULATION TECHNIQUES.(U)
DEC 78 J L CRADDOCK

UNCLASSIFIED AFIT/GE/EE/78-23 NL

2 OF 2
AD
A064363



END
DATE
FILMED
4 -79
DDC


1.0
1.1
1.25
1.4
1.6
1.8
2.0
2.2
2.5
2.8
3.2
3.6
4.0
4.5
5.0
MICROCOPY RESOLUTION TEST CHART
NATIONAL BUREAU OF STANDARDS-1963-A

24. Greenstein, L.J. "Spectra of PSK Signals with Overlapping Baseband Pulses," IEEE Transactions on Communications, COM-25 5:523-530 (May 1977).

25. Kwan, Robert K. "The Effects of Filtering and Limiting A Double-Binary PSK Signal," IEEE Transactions on Aerospace Electronic Systems, AES-5: 589-594 (July 1969).

26. Thomas, John B. An Introduction to Statistical Communication Theory. New York: John Wiley & Sons, Inc., 1969.

27. Nielson, Wade L. and Stanley R. Robinson. "Quadrature Clock Modulation for Improved Binary Communication in the Presence of Intersymbol Interference," Proceedings of International Conference on Communications. 21.3/91-95. Chicago, Illinois: IEEE, June 1977.

28. Wozencraft, J.M. and J.R. Jacobs. Principles of Communication Engineering. New York: John Wiley & Sons, Inc., 1965.

29. Fielding, R.M., H.L. Berger and D.L. Lochhead. "Performance Characterization of a High Data Rate MSK and QPSK Channel," Proceedings of International Conference on Communications. 3.2/42-26. Chicago, Illinois: IEEE, June 1977.

30. Kalet, Irving and Brian E. White. "Suboptimal Continuous Shift Keyed (CSK) Demodulation for the Efficient Implementation of Low Crosstalk Data Communication," IEEE Transactions on Communications, COM-25 9: 1037-1041 (September 1977).

31. White, Brian E., Irvin Kalet and Harold M. Heggestad. "Offset Quadrature Phase Comparison Modulation Schemes for Low Crosstalk Communication," Proceedings of International Conference on Communications. 6.5/133-137. Chicago, Illinois: IEEE, June 1977.

32. Metzger, Louis S. "Performance of Phase Comparison Sinusoidal Frequency Shift Keying," IEEE Transactions on Communications, COM-26 8: 1250-1253 (August 1978).

VITA

Joseph L. Craddock was born on 5 September 1945 in Klamath Falls, Oregon. He graduated from Butte Valley High School, Dorris, California in 1963 and attended Oregon Institute of Technology, Klamath Falls, Oregon, from which he received the degree of Bachelor of Technology in Electrical Engineering Technology in June 1969. After graduation, he worked for Cintra Electronics in Mountain View, California, until he entered the Air Force in November 1969. He received an AF Commission through Officers Training School (OTS) in February 1970, and was assigned to Keesler Technical Training Center, Keesler AFB, Mississippi, where he attended the Communications Maintenance Officers Course (30BR3031). Upon graduation from this school, he was awarded the 3031 and 3051 AFSCs and assigned as the Maintenance Control OIC at the 1911 Communications Squadron (AFCS), Offutt AFB, Nebraska. In 1972 he was assigned as the Detachment Communications Electronics Systems Maintenance Engineer at Detachment 28 of the 2187 Communications Group (AFCS), Mt. Vergine, Italy. This was followed in 1974 by an assignment to AFCS/EPE, Richards-Gebaur AFB, Missouri, as a MAJCOM Electrical Engineer until he entered the Air Force Institute of Technology post graduate engineering program in June 1976 to persue studies in communications and digital signal processing.

Permanent address: 530 Juniper Street
Chico, California 95926

UNCLASSIFIED

SECURITY CLASSIFICATION OF THIS PAGE (When Data Entered)

REPORT DOCUMENTATION PAGE	READ INSTRUCTIONS BEFORE COMPLETING FORM
1. REPORT NUMBER (14) AFIT/GE/EE/78-23 ✓	2. GOVT ACCESSION NO. (9) Master's thesis ✓
4. TITLE (and Subtitle) (6) ANALYSIS OF MODERN DIGITAL MODULATION TECHNIQUES. ✓	5. TYPE OF REPORT & PERIOD COVERED: MS Thesis
	6. PERFORMING ORG. REPORT NUMBER
7. AUTHOR(s) (10) Joseph L. Craddock Capt USAF	8. CONTRACT OR GRANT NUMBER(s)
9. PERFORMING ORGANIZATION NAME AND ADDRESS: Air Force Institute of Technology (AFIT-EN) Wright-Patterson AFB, Ohio 45433	10. PROGRAM ELEMENT, PROJECT, TASK AREA & WORK UNIT NUMBERS: (16) 63727F 2277
11. CONTROLLING OFFICE NAME AND ADDRESS: Rome Air Development Center/DCID Griffis AFB, NY 13441	12. REPORT DATE: (11) 15 December 1978 13. NUMBER OF PAGES: 98
14. MONITOPING AGENCY NAME & ADDRESS(if different from Controlling Office) (12) 100p.	15. SECURITY CLASS. (of this report): Unclassified 15a. DECLASSIFICATION/DOWNGRADING SCHEDULE

16. DISTRIBUTION STATEMENT (of this Report)

Apprcved for public release; distribution unlimited.

17. DISTRIBUTION STATEMENT (of the abstract entered in Block 20, if different from Report)

18. SUPPLEMENTARY NOTES: Approved for public release; IAW AFR 190-17

JOSEPH P. HIPPS, Major USAF
Director of Information 1-23-79

19. KEY WORDS (Continue on reverse side if necessary and identify by block number)

Frequency Modulation
Phase Modulation
Narrowband
Power Spectra

20. ABSTRACT (Continue on reverse side if necessary and identify by block number)

Offset Quadriphase Shift Keyed (OQPSK) modulation, Minimum Shift Keyed (MSK) modulation and Sinusoidal Frequency Shift Keyed (SFSK) modulation are analyzed and compared within this report. First, OQPSK, MSK and SFSK are examined both graphically and mathematically, and compared to the fundamental modulation techniques of FSK, PSK and QPSK. Second, a common mathematical framework unifying the three modulation techniques is developed. Third, the theoretical spectral properties of each are calculated.)

DD FORM 1 JAN 73 1473 EDITION OF 1 NOV 65 IS OBSOLETE

Next page

UNCLASSIFIED

SECURITY CLASSIFICATION OF THIS PAGE (When Data Entered)

012 225

20. (Abstract continued)

The spectral properties include the autocorrelation function, power spectral density, spectral occupancy, spectral shape and roll off characteristics. Next, the practical spectral properties of the three modulation techniques are developed using a realistic bandlimited, nonlinear channel. Finally, simulated and measured performance of OQPSK and MSK are given and compared using probability of error as the figure of merit.